

PROJECT SUMMARY: Multiscale Homogenization for Sea Ice

The precipitous loss of Arctic sea ice observed in the past few decades has far reaching impact on the polar marine environment as well as more broadly on Earth's climate system. This reduced ice cover also opens up new opportunities for navigation, exploration and extraction of energy and food resources, and increased human activity in general. Along with the Arctic opening up goes the potential for more interactions and competition between countries. Thus it is of strategic as well as scientific interest to improve projections of how the sea ice cover may evolve in the future, and to develop more rigorous representations of sea ice in predictive models of the climate system and marine environment.

One of the fundamental challenges of modeling sea ice and climate is to account for important processes that occur on scales finer than the coarse grids of numerical models, and how they influence larger scale effective behavior of the system. This *linkage of scales* is particularly interesting, relevant – and challenging – for sea ice, as it exhibits composite structure on length scales ranging over many orders of magnitude. Millimeter scale brine inclusions are laced throughout the ice, and coalesce to form meter scale channels through which fluid can flow. Sea ice has centimeter scale polycrystalline structure which helps determine its bulk fluid flow and mechanical properties. Convective brine flows with meter scale structure affect bulk thermal and nutrient transport. Sea ice floes ranging from a few centimeters to tens of kilometers form the *microstructure* of the sea ice pack, viewed from an aircraft or satellite as a time-evolving composite of ice and ocean. The Arctic sea ice surface in late spring and summer is a complex mosaic of snow and pools of melt water on meter to kilometer scales, which determine sea ice albedo, a critical parameter in climate models.

Here we propose to develop powerful methods of homogenization, over a broad range of scales as indicated above, to accurately account for important *sub-grid scale* sea ice structures and processes in climate modeling. We consider several key issues critical to advancing predictive capability, where mathematics of homogenization and statistical physics can provide a rigorous framework for analysis and computation. They include:

- **Advection diffusion processes.** Develop bounds and spectral measure computations for advection enhanced diffusivity, such as the thermal conductivity of sea ice in the presence of convection, or the diffusion coefficient of a tagged floe in the ice pack. Develop inverse methods for recovering diffusion and velocity fields in large scale, effective advection diffusion models of sea ice evolution.
- **Ocean waves in sea ice.** Develop bounds on the effective complex viscoelasticity of the sea ice layer for wave propagation in the marginal ice zone (MIZ), via Stieltjes integrals with *spectral measures* which depend on floe geometry and configurations.
- **Low order predictors.** Explore the use of simplified partial differential equation models for analyzing and predicting fundamental characteristics of the sea ice pack, such as MIZ width and sea ice concentration in unobserved regions.
- **Statistical physics of melt ponds.** Analyze critical exponents of melt pond evolution as long range order or connectivity develops, such as the correlation length exponent. Develop an Ising model of melt pond geometry that incorporates ice-albedo feedback, and investigate other low order models of melt pond and albedo evolution.

TECHNICAL PROPOSAL

ONR BAA Announcement Number: N00014-17-S-B001

ONR Applied Computational Analysis Program

Multiscale Homogenization for Sea Ice

Principal Investigator: Kenneth M. Golden*

Co-Principal Investigators: Elena Cherkaev[†]
Courtenay Strong[‡]

Administrative/Business Contact: Shauna Peterson[§]

November 1, 2017 – October 31, 2020

*University of Utah, Department of Mathematics, 155 S 1400 E, RM 233, Salt Lake City, UT 84112-0090, Tel: 801-581-6176, Fax: 801-581-4148, Email: golden@math.utah.edu

[†]University of Utah, Department of Mathematics, 155 S 1400 E, RM 233, Salt Lake City, UT 84112-0090, Tel: 581-7315, Fax: 801-581-4148, Email: elena@math.utah.edu

[‡]University of Utah, Department of Atmospheric Sciences, 135 S 1460 E, RM 819, Salt Lake City, Utah 84112-0110, Tel: 801-585-0049, Fax: 801-585-3681, Email: court.strong@utah.edu

[§]1471 East Federal Way, Salt Lake City, UT 84112-0090, Tel: 801-585-0062, Fax: 801-581-3007, shauna.peterson@osp.utah.edu

Contents

1	Technical Approach	1
1.1	Introduction	1
1.2	Mathematical Models of Composites and Phase Transitions	2
1.2.1	Percolation models	2
1.2.2	Homogenization and spectral measures	4
1.2.3	Phase transitions and the Ising model of a ferromagnet.	6
1.3	Stieltjes integral representations for sea ice parameters	6
1.3.1	Electromagnetic behavior of polycrystalline materials.	6
1.3.2	Advection diffusion and thermal conductivity of sea ice	8
1.3.3	Fluid permeability and the trapping constant	10
1.3.4	Complex viscoelasticity for wave propagation in the marginal ice zone	12
1.4	Low order models and large scale advection diffusion	15
1.4.1	Advection diffusion in the marginal ice zone	15
1.4.2	Inversion of the concentration field for spatially varying diffusivity . .	17
1.4.3	Filling the polar data gap	18
1.4.4	Anomalous diffusion in the marginal ice zone	20
1.5	Statistical physics of melt pond evolution	21
1.5.1	Percolation theory for melt ponds	22
1.5.2	Ising model for melt ponds	25
1.6	References	27
2	Management Approach	36
3	Current and Pending Projects and Proposals	38
4	Qualifications	43

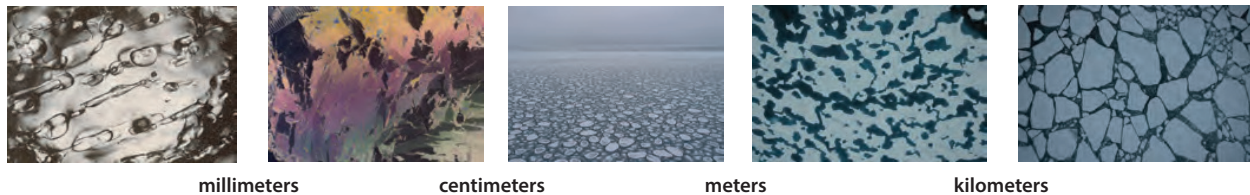


Figure 1: **Multiscale structure of sea ice.** From left to right: sub–millimeter scale brine inclusions that form the porous microstructure of sea ice [122]; centimeter scale polycrystalline structure of sea ice [1]; decimeter to meter scale pancakes forming in a wave field in the Southern Ocean (Golden); melt ponds on the scale of decimeters to kilometers on the surface of Arctic sea ice in late spring and summer (Perovich); kilometer scale floes in the Arctic sea ice pack (Perovich) exhibit local diffusion in their interactions with other floes and can be advected in larger scale wind and current fields with coherent structure on the scale of hundreds of kilometers.

1 Technical Approach

1.1 Introduction

One of the fascinating, yet challenging aspects of modeling sea ice and its role in global climate is the sheer range of relevant length scales of structure – over ten orders of magnitude, from the sub-millimeter scale to hundreds of kilometers, as indicated in Figure 1. Modeling sea ice on scales appropriate for global climate models depends on an understanding of the physical properties of sea ice at the scale of individual floes and even down to the scale of brine inclusions which control so many of these properties. Climate models challenge the most powerful supercomputers to their fullest capacity. However, even the largest computers still limit the horizontal resolution to tens of kilometers and typically require clever approximations and parameterizations to model the basic physics of sea ice.

A central theme of our proposed work is how to use information about smaller scales to predict effective behavior on larger scales. We observe here that this central problem of climate science shares commonality with the key challenges, for example, of statistical mechanics where knowledge of molecular interactions is used to derive collective or macroscopic behavior. Moreover, it also shares fundamental similarities with homogenization theory for composites where larger scale effective properties are calculated from knowledge of the microstructure. These fields of physics and applied mathematics provide a natural – and powerful – framework for advancing how we treat sea ice in predictive models of climate, and improving projections of how Earth’s polar ice packs may evolve in the future.

In particular, the analytic continuation method [9, 77, 41, 44, 79] yields powerful integral representations for the effective or homogenized transport coefficients of two [41] or multi-phase [42, 38] composite materials. The method exploits the properties of these coefficients as analytic functions of the system parameters, such as ratios of the conductivities of the phases. The geometry of the composite microstructure is encoded into a *spectral measure* of a random self adjoint operator G , the key object in the method. Because of the Stieltjes form of the integral representation, knowing moments of the measure – or information about the composite microstructure – yields rigorous bounds on the homogenized trans-

port coefficient [5, 38]. Moreover, in a discrete model of the composite, the operator G becomes a random matrix, whose eigenvalues and eigenvectors can be used to compute the spectral measure. The *microscale* structure, which determines the spectral measure and the homogenized coefficient, is thus linked to the *macroscopic* behavior via the operator G .

Here we propose to develop this powerful approach in contexts beyond transport in two phase composites, that are motivated by considerations of the role of sea ice in the climate system over a broad range of scales. In so doing, we will significantly advance our ability to rigorously account for sub-grid scale structures and processes in predictive models. In particular, we will develop Stieltjes integral approaches to the following homogenization problems for sea ice: its polycrystalline structure, advection diffusion processes such as the thermal conductivity in the presence of fluid convection, the *trapping constant* of a porous medium which is related to the fluid permeability, and ocean waves propagating through the marginal ice zone (MIZ). All these problems are put on an equal footing via a resolvent representation for the relevant local field in each case, such as the electric or strain field.

Moreover, we will explore larger scale homogenization problems such as finding low order partial differential equation models of sea ice evolution. For example, solutions of Laplace’s equation have been very useful in objectively measuring the width of the MIZ and its recent widening [105, 109, 106], and filling in the so-called *polar data gap* [107, 108]. Natural generalizations of these simplistic models include a spatially dependent diffusion coefficient, sources and sinks, and an advective flow field. We will develop numerical models of floe aggregates which can be used to investigate diffusion of individual floes, *jamming states* which may lead to sub-diffusive behavior, and the homogenized problem. Finally we will investigate melt ponds from a percolation theory viewpoint, and continue development of an Ising model approach to understanding the evolution of melt pond geometry.

1.2 Mathematical Models of Composites and Phase Transitions

Here we give a brief overview of some of the mathematical models and ideas that we will use in developing homogenization schemes for linking scales in the sea ice – climate system.

1.2.1 Percolation models

Sea ice is a porous composite of pure ice with liquid brine inclusions. These inclusions host extensive algal and bacterial communities which support life in the polar oceans [111, 37]. The flow of fluids through sea ice mediates processes important to climate such as melt pond drainage, which is critical to the evolution of sea ice albedo. Fluid flow through sea ice also governs the evolution of the salt budget and salinity profiles [111], convection-enhanced thermal transport [69], ocean-ice-atmosphere CO₂ exchanges [98], and the build-up of algal biomass fueled by fluxes of nutrients [111, 37]. It also drives snow-ice formation, which accounts for a significant portion of the ice produced in the Southern Ocean [72]. Sea water percolates upward through the porous brine microstructure, flooding the snow layer, which subsequently freezes.

Sea ice exhibits a very interesting and important critical phenomenon [47]. For brine volume fractions ϕ below about 5%, columnar sea ice is effectively impermeable to fluid flow, while for ϕ above 5%, it is increasingly permeable. The critical brine volume fraction

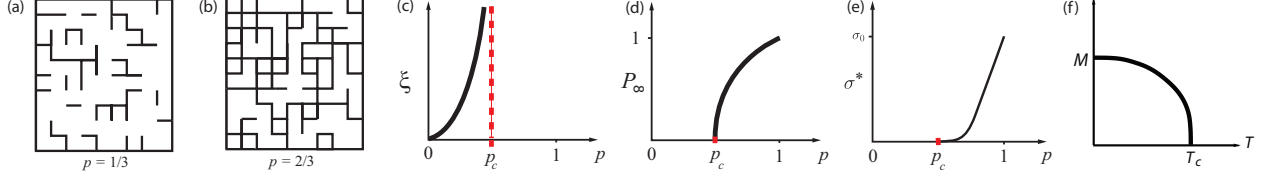


Figure 2: The two dimensional square lattice percolation model below its percolation threshold of $p_c = 1/2$ in (a) and above it in (b). (c) Divergence of the correlation length as p approaches p_c . The infinite cluster density of the percolation model is shown in (d), and the effective conductivity is shown in (e). (f) The magnetization of the Ising model.

$\phi_c \approx 5\%$ corresponds to a critical temperature $T_c \approx -5^\circ$ for a typical bulk sea ice salinity of 5 parts per thousand. This critical behavior in the fluid flow properties of sea ice, occurring at this particular threshold, is known as the *rule of fives*. Given the broad range of processes which are governed by fluid flow through the porous microstructure of the ice, this rule can be thought of, roughly speaking, as the *on-off switch* for fluid flow in sea ice. Understanding how the fluid permeability of sea ice depends on temperature T or brine volume fraction ϕ is prerequisite to incorporating processes governed by fluid flow into climate models. In [47] we showed how this *on-off switch* can be explained in terms of percolation theory, which we now discuss.

Consider the d -dimensional integer lattice \mathbb{Z}^d , and the square or cubic network of bonds joining nearest neighbor lattice sites. In the percolation model [16, 103, 51, 18], we assign to each bond a conductivity $\sigma_0 > 0$ with probability p , meaning it is open (black), and with probability $1-p$ we assign a 0, meaning it is closed. Two examples of lattice configurations are shown in Figure 2, with $p = 1/3$ in (a) and $p = 2/3$ in (b). Groups of connected open bonds are called *open clusters*. In this model there is a critical probability p_c , $0 < p_c < 1$, called the *percolation threshold*, at which the average cluster size diverges and an infinite cluster appears. For the two dimensional bond lattice $p_c = 1/2$. For $p < p_c$ the density of the infinite cluster $P_\infty(p)$ is 0, while for $p > p_c$, $P_\infty(p) > 0$ and near the threshold, $P_\infty(p) \sim (p - p_c)^\beta$ as $p \rightarrow p_c^+$, where β is a universal critical exponent, that is, it depends only on dimension and not on the details of the lattice. Let $x, y \in \mathbb{Z}^d$ and $\tau(x, y)$ be the probability that x and y belong to the same open cluster. Then for $p < p_c$, $\tau(x, y) \sim e^{-|x-y|/\xi(p)}$, and the correlation length $\xi(p) \sim (p_c - p)^{-\nu}$ diverges with a universal critical exponent ν as $p \rightarrow p_c^-$, as shown in Figure 2 (c).

The effective conductivity $\sigma^*(p)$ of the lattice, now viewed as a random resistor (or conductor) network, defined via Kirchoff's laws, vanishes for $p < p_c$ like $P_\infty(p)$ since there are no infinite pathways, as shown in Figure 2 (e). For $p > p_c$, $\sigma^*(p) > 0$, and near p_c , $\sigma^*(p) \sim \sigma_0(p - p_c)^t$, $p \rightarrow p_c^+$, where t is the conductivity critical exponent, with $1 \leq t \leq 2$ in $d = 2, 3$ (for an idealized model) [39, 40, 45], and numerical values $t \approx 1.3$ in $d = 2$ and $t \approx 2.0$ in $d = 3$ [103]. Consider a random pipe network with effective fluid permeability $\kappa^*(p)$ exhibiting similar behavior $\kappa^*(p) \sim \kappa_0(p - p_c)^e$, where e is the permeability critical exponent, with $e = t$ [19, 100, 45]. Both t and e are believed to be universal – they depend only on dimension and not the lattice. Continuum models can exhibit nonuniversal behavior with exponents different from the lattice case and $e \neq t$ [53, 35, 103, 99, 61].

1.2.2 Homogenization and spectral measures

Homogenization denotes a field of applied mathematics where the goal is to find a homogeneous medium which behaves macroscopically the same as a given inhomogeneous medium. The methods are focused on finding the effective properties of inhomogeneous media such as composites. We will see that the *spectral measure* provides a powerful tool for upscaling geometrical information about a composite into calculations of effective properties.

We now briefly describe the *analytic continuation method* for studying the effective properties of composite materials [9, 77, 41, 44]. This method has been used to obtain rigorous bounds on effective transport coefficients of composite materials from partial knowledge of the microstructure, such as the relative volume fractions of the phases. Later we will show how this method may be adapted to studies of polycrystalline media [52, 6], advection-enhanced diffusion processes [2, 3, 86, 87], thermal transport in sea ice enhanced by brine convection, and wave propagation in the MIZ.

For simplicity we choose the electrical conductivity of a two-phase composite, although the method applies to any classical transport coefficient. Consider a two-phase random medium with local conductivity tensor $\sigma(x, \omega)$, a spatially stationary random field in $x \in \mathbb{R}^d$ and $\omega \in \Omega$, where Ω is the set of realizations of the medium. Later, we will consider a polycrystalline medium where σ is a non-trivial symmetric matrix. Here we consider a two-phase locally isotropic medium, where $\sigma(x, \omega) = \sigma(x, \omega)I$, I is the identity matrix, and

$$\sigma(x, \omega) = \sigma_1 \chi_1(x, \omega) + \sigma_2 \chi_2(x, \omega). \quad (1)$$

Here $\chi_j(x, \omega)$ is the characteristic function of medium $j = 1, 2$, equaling 1 for $\omega \in \Omega$ with medium j at x , and 0 otherwise. Let $E(x, \omega)$ and $J(x, \omega)$ be the stationary random electric and current fields, satisfying

$$\nabla \times E = 0, \quad \nabla \cdot J = 0, \quad J = \sigma E, \quad \langle E \rangle = e_k, \quad (2)$$

where $\langle \cdot \rangle$ is ensemble averaging over Ω or spatial average over all of \mathbb{R}^d [41]. For simplicity, we have set the magnitude of $\langle E \rangle$ to 1 and its direction e_k is a standard basis vector in the k th direction. The effective conductivity tensor σ^* is defined as

$$\langle J \rangle = \sigma^* \langle E \rangle. \quad (3)$$

We focus on one diagonal coefficient $\sigma^* = \sigma_{kk}^*$, with $\sigma^* = \langle \sigma E \cdot e_k \rangle$, and since σ^* depends on $h = \sigma_1/\sigma_2$, we define $m(h) = \sigma^*/\sigma_2$, which is a Stieltjes function. It is analytic off $(-\infty, 0]$ in the complex h -plane, and maps the upper half plane to the upper half plane [8, 41].

The key step [41, 8, 77, 79] is to obtain an integral representation for σ^* . Consider $F(s) = 1 - m(h)$, $s = 1/(1 - h)$, which is analytic off $[0, 1]$ in the s -plane. Then [41]

$$F(s) = 1 - \frac{\sigma^*}{\sigma_2} = \int_0^1 \frac{d\mu(\lambda)}{s - \lambda}, \quad s = \frac{1}{1 - \sigma_1/\sigma_2}, \quad (4)$$

where μ is a positive measure on $[0, 1]$. This formula arises from a resolvent representation of the electric field (in medium 1),

$$\chi_1 E = s(sI - G)^{-1} \chi_1 e_k, \quad G = \chi_1 \Gamma \chi_1, \quad (5)$$

yielding $F(s) = \langle [(s - \chi_1 \Gamma \chi_1)^{-1} \chi_1 e_k] \cdot e_k \rangle$, where $\Gamma = -\nabla(-\Delta)^{-1}\nabla \cdot$ and $\Delta = \nabla^2$ is the Laplacian. In the Hilbert space $L^2(\Omega)$, the operator $G = \chi_1 \Gamma \chi_1$ is self adjoint. Formula (4) is the spectral representation of the resolvent and μ is a spectral measure of $G = \chi_1 \Gamma \chi_1$.

Formula (4) separates the component parameters in s from the geometrical information in μ . (Extensions to multicomponent media involve several complex variables [42, 38, 81, 78, 29].) Information about the geometry enters through the moments

$$\mu_n = \int_0^1 \lambda^n d\mu(\lambda) = \langle G^n e_k \cdot e_k \rangle, \quad (6)$$

Then $\mu_0 = \phi$, where ϕ is the volume or area fraction of phase 1, such as the melt pond coverage, and $\mu_1 = \phi(1 - \phi)/d$ if the material is statistically isotropic. In general, μ_n depends on the $(n + 1)$ -point correlation function of the medium. This integral representation yields rigorous *forward bounds* for the effective parameters of composites, given partial information on the microgeometry via the μ_n [9, 77, 41, 10]. One can also use the integral representations to obtain *inverse bounds*, allowing one to use data about the electromagnetic response of a sample, for example, to bound its structural parameters, such as the volume fraction of each of the components [74, 75, 23, 20, 24, 124, 14, 22, 28, 50].

In the discrete setting of a square lattice, the action of the operator G is given by that of a real-symmetric *random matrix* M , where Γ is a (non-random) projection matrix which depends only on the lattice topology and boundary conditions, and χ_1 is a diagonal (random) projection matrix which determines the geometry and component connectivity of the composite medium [85]. In this setting, $\chi_1 E$ and the integral in equations (5) and (4) have explicit representations in terms of the eigenvalues λ_i and eigenvectors u_i of M [85]

$$\chi_1 E = s \sum_i \frac{\sqrt{m_i}}{s - \lambda_i} u_i, \quad F(s) = \sum_i \left\langle \frac{m_i}{s - \lambda_i} \right\rangle, \quad m_i = |u_i \cdot \chi_1 \hat{e}_k|^2, \quad (7)$$

where \hat{e}_k plays the role of a standard basis vector on the lattice. This shows the discrete spectral measure μ is given explicitly in terms of the eigenvalues λ_i and orthonormal eigenvectors u_i of the matrix M [85]:

$$\mu(d\lambda) = \langle Q(d\lambda) \hat{e}_k \cdot \hat{e}_k \rangle, \quad Q(d\lambda) = \sum_i \delta_{\lambda_i}(d\lambda) \chi_1 Q_i, \quad Q_i = u_i u_i^T. \quad (8)$$

Here, $Q(d\lambda)$ is the projection valued measure associated with M , $\delta_{\lambda_i}(d\lambda)$ is the delta measure centered at λ_i , and the matrix $Q_i = u_i u_i^T$ is a projection onto the eigenspace spanned by u_i [85]. In the continuum setting, the spectral measure of G still has the form $\mu(d\lambda) = \langle Q(d\lambda) e_k \cdot e_k \rangle$ but $Q(d\lambda)$ is abstract in nature and is not given explicitly as in (8) [104].

To compute μ a non-standard generalization of the spectral theorem for matrices is required, due to the projective nature of the matrices χ_1 and Γ [85]. In particular, we developed a *projection method* that demonstrates the spectral measure μ in (8) depends only on the eigenvalues and eigenvectors of random sub-matrices of Γ of size $N_1 \approx \phi N$ corresponding to diagonal components $[\chi_1]_{ii} = 1$ [85]. Moreover for the periodic setting, the matrix Laplacian is singular so the matrix representation of $(-\Delta)^{-1}$ is not defined. We have recently extended the results in [85] to the periodic setting, utilizing properties of the singular value decomposition (SVD) of the matrix gradient ∇ . This extension not only alleviated the issues associated with the 3D RRN discussed in [85] but also gave rise to new spectral behaviors not previously discovered in related numerical investigations [59].

1.2.3 Phase transitions and the Ising model of a ferromagnet.

The Ising model of a ferromagnet in a magnetic field H and at temperature T is perhaps the most studied example of a phase transition in statistical mechanics [112, 26, 43]. We consider a finite box $\Lambda \subset \mathbb{Z}^d$ containing N sites. At each site there is a spin variable s_i which can take the values $+1$ or -1 . We consider a Hamiltonian with ferromagnetic pair interaction $J \geq 0$ between nearest neighbor pairs $\langle i, j \rangle$,

$$\mathcal{H}_\omega = -H \sum_i s_i - J \sum_{\langle i, j \rangle} s_i s_j, \quad (9)$$

for any configuration $\omega \in \Omega = \{-1, 1\}^N$ of the spins. The average magnetization, which serves as the principal *order parameter* in the system, $M(T, H) = \lim_{N \rightarrow \infty} \frac{1}{N} \langle \sum_{i=1}^N s_i \rangle$, where $\langle \cdot \rangle$ in this context denotes averaging over $\omega \in \Omega$ with Gibbs weights, can be expressed in terms of the free energy (per unit site) f as $M(T, H) = -\frac{\partial f}{\partial H}$. The magnetic susceptibility $\chi(T, H)$, which is the analog of the effective conductivity in Section 1.2.2, is given by $\chi(T, H) = \frac{\partial M}{\partial H} = -\frac{\partial^2 f}{\partial H^2} \geq 0$. When $H = 0$, $M(T) \sim (T_c - T)^\beta$ as $T \rightarrow T_c^-$, as shown in Figure 2 (f), and $\chi \sim (T - T_c)^{-\gamma}$ as $T \rightarrow T_c^+$. The universal exponent β here plays a similar role as β for the percolation model, but has a different numerical value. Below we will discuss how this framework can be used to model melt ponds.

Principal Scientific Investigations

1.3 Stieltjes integral representations for sea ice parameters

1.3.1 Electromagnetic behavior of polycrystalline materials.

Our recent paper [52] and new analysis (below) of the electromagnetic transport properties of random, uniaxial polycrystalline media has demonstrated that the underlying, rigorous mathematical framework is a direct analogue of that for two-phase random media described in Section 1.2.2. For simplicity, we discuss the theory in terms of conductive polycrystalline materials, which are composed of many crystallites (single crystals of varying size, shape, and orientation) that can have different local conductivities along different crystal axes. The second panel in Figure 1 displays the polycrystalline structure of sea ice and Figure 3 (a) displays a numerically generated polycrystalline structure. In the case of uniaxial polycrystalline media, the local conductivity along one of the crystal axes has the *complex* value σ_1 , while the conductivity along all the other crystal axes have the value σ_2 . The local conductivity tensor of such media is given by [80, 6] $\boldsymbol{\sigma}(x, \omega) = R^T \text{diag}(\sigma_1, \sigma_2, \dots, \sigma_2) R$, where $R(x, \omega)$ is a random rotation matrix, and $\boldsymbol{\sigma}$ can be written in a form which is a direct analogue of (1), involving the matrices $C = \text{diag}(1, 0, \dots, 0)$ and $X_1 = R^T C R$,

$$\boldsymbol{\sigma}(x, \omega) = \sigma_1 X_1(x, \omega) + \sigma_2 X_2(x, \omega), \quad (10)$$

where X_1 is a random projection matrix, $X_2 = I - X_1$, $X_j X_k = X_i \delta_{jk}$, $j, k = 1, 2$, and δ_{jk} is the Kronecker delta.

The propagation properties of a quasistatic electromagnetic wave in a polycrystalline medium are determined by (2) (or analog $D = \epsilon E$ for permittivity), and the effective complex

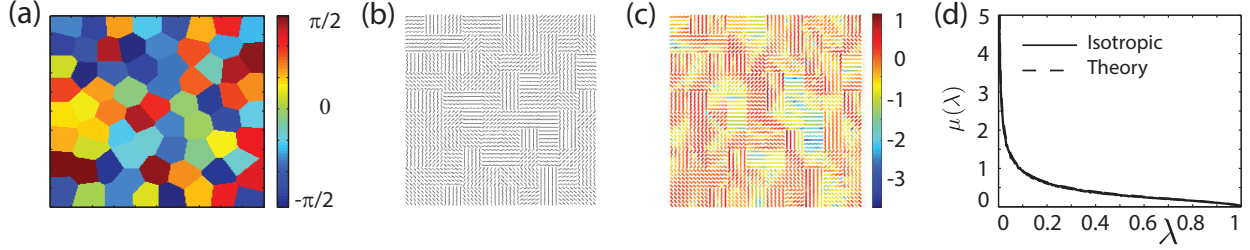


Figure 3: *Spectral analysis of polycrystalline media.* (a) Geometric shapes generated using a Voronoi diagram, with orientation angles uniformly distributed on the interval $(-\pi/2, \pi/2)$. (b) A graphical, lattice representation of a polycrystalline medium which is isotropic within the horizontal plane, having checkerboard microstructure comprised of squares with 5 grid points in length. (c) Electric fields for the polycrystalline microstructure in (b) computed via equation (7). (d) Spectral function $\mu(\lambda)$ (histogram representations of the spectral measure) for the polycrystalline microstructure described in (b) computed via equation (8). The spectral function $\mu(\lambda)$ is displayed with its isotropic theoretical prediction [79] $\mu_I(\lambda) = (\sqrt{(1-\lambda)/\lambda})/\pi$.

conductivity tensor σ^* is defined by (3). Moreover, in precise parallel with the two component setting, writing equation (10) as $\sigma = \sigma_2(I - X_1/s)$ yields $X_1 E = s(sI - X_1 \Gamma X_1)^{-1} X_1 e_k$, an analogue of (5). A Stieltjes integral representation for the diagonal component $\sigma_k^* = \sigma_{kk}^*$ of σ^* , is given by equation (4) with $F(s) = \langle [(sI - X_1 \Gamma X_1)^{-1} X_1 e_k] \cdot e_k \rangle$. Furthermore, the positive *spectral measure* μ on $[0, 1]$ is given by $\mu(d\lambda) = \langle Q(d\lambda) X_1 e_k \cdot e_k \rangle$ and $Q(d\lambda)$ is the projection valued measure associated with the random, bounded, self-adjoint operator $X_1 \Gamma X_1$ on $L^2(\Omega)$ with moments μ_n given by (6) with $G = X_1 \Gamma X_1$. The mass $\mu_0 = \langle X_1 e_k \cdot e_k \rangle$ of μ can be thought of as the percentage of the crystals oriented in the k th direction e_k [52, 6].

In the discrete setting, the electric field $X_1 E$ and the summation formula for $F(s)$ in equation (7) still hold for polycrystalline media, where λ_i and u_i are the eigenvalues and eigenvectors of the random matrix $M = X_1 \Gamma X_1$. The discrete spectral measure is also given by equation (7) with X_1 in place of χ_1 . We have developed a projection method for direct computation of spectral measures, conductivities, and fields via analogues of equations (7) and (8); see Fig. 3 (b)-(d).

We propose to directly compute spectral measures, corresponding effective transport parameters, and fields for various polycrystalline microstructures. These media include random checkerboards (shown in Fig. 3(b) and (c) and more realistic microstructures such as that displayed in Fig. 3(a) with various crystallite orientation statistics. We will investigate the associated electromagnetic transport properties of sea ice as a polycrystalline medium, with particular focus on columnar vs. granular microstructures, which have different fluid flow characteristics. Electromagnetically distinguishing between these two ice types is of particular interest. We will also explore the possible characterization of crystallite microstructures by geometric resonances in the measures, and transitions in the transport properties by behavior of spectral gaps, eigenvalue correlations, and eigenvector localization properties, which play a key role in the effective properties of two-component composites [84, 85]. An extension of the spectral coupling [20, 21, 25, 22] in two component composites to polycrystalline media is also of key interest, so as to recover from the computed spectral measures,

the electromagnetic and thermal transport properties of polycrystalline sea ice.

1.3.2 Advection diffusion and thermal conductivity of sea ice

The enhancement of diffusive transport of passive scalars by complex fluid flow plays a key role in many important processes in the global climate system [120] and Earth's ecosystems [31]. Advection of geophysical fluids intensifies the dispersion and large scale transport of heat [82], pollutants [27, 11, 101], and nutrients [31, 55] diffusing in their environment. In sea ice dynamics, where the ice cover couples the atmosphere to the polar oceans [120], the transport of sea ice can also be enhanced by eddy fluxes and large scale coherent structures in the ocean [121, 67]. In sea ice thermodynamics, the temperature field of the atmosphere is coupled to the temperature field of the ocean through sea ice, a composite of pure ice with brine inclusions whose volume fraction and connectedness depend strongly on temperature [111, 48, 46]. Convective brine flow through the porous microstructure can enhance thermal transport through the sea ice layer [69, 123, 64].

The effective parameter problem for two-component composites discussed in Section 1.2.2 reduces the analysis of complex composite materials, with rapidly varying structures in space, to solving averaged, or *homogenized* equations that do not have rapidly varying data, and involve an effective parameter. This mathematical framework was extended [73, 71] to homogenize the advection diffusion equation, involving a complex fluid velocity field with rapidly varying structures in both space and time, yielding a homogenized equation involving an effective diffusivity tensor \mathbf{D}^* . Moreover, a Stieltjes integral representation of \mathbf{D}^* was obtained [2, 3, 86, 87, 91, 4, 12], which involves a spectral measure ν of a self-adjoint, Hermitian operator (or matrix). This representation separates the molecular diffusivity (or equivalently the Péclet number) from the geometric complexity and dynamics of the flow [86, 87], which is incorporated in the moments $\nu_n = \int \lambda^n d\nu(\lambda)$ of the measure ν . As in the setting of composite media, Padé approximants provide rigorous bounds on the components of \mathbf{D}^* involving the moments ν_n [5, 3]. The bounds get progressively tighter as additional moments are incorporated. We now review this mathematical framework in terms of enhanced thermal conductivity in the presence of a brine velocity field. This framework can also be used to model the advection enhanced dispersion of sea ice floes by atmospheric winds and oceanic currents collectively giving rise to a transporting flow.

The enhancement of sea ice thermal conductivity κ by a space-time periodic brine velocity field u , above the value κ_0 of sea ice with no fluid flow, is described by the advection-diffusion equation

$$\rho c [\partial_t T + \phi u \cdot \nabla T] = \kappa_0 \Delta T, \quad T(0, x) = T_0(x). \quad (11)$$

Here, $\kappa_0 = 2 \text{ W/(m K)}$, $\rho = 960 \text{ kg/m}^3$ is the bulk density of sea ice, $c = 2.11 \text{ J/(g K)}$ is the specific heat, and ϕ is the brine volume fraction - a function of T itself in reality, though taken here as an independent parameter here for simplicity. Moreover, the *bulk* brine velocity field $u(t, x)$ and the initial value $T_0(x)$ of the temperature $T(t, x)$ are given, u is incompressible, $\nabla \cdot u = 0$, and ∂_t denotes differentiation with respect to time t .

Non-dimensionalizing and homogenizing (11) shows [73] that the effective behavior of thermal transport in sea ice is described by a diffusion equation involving an averaged tem-

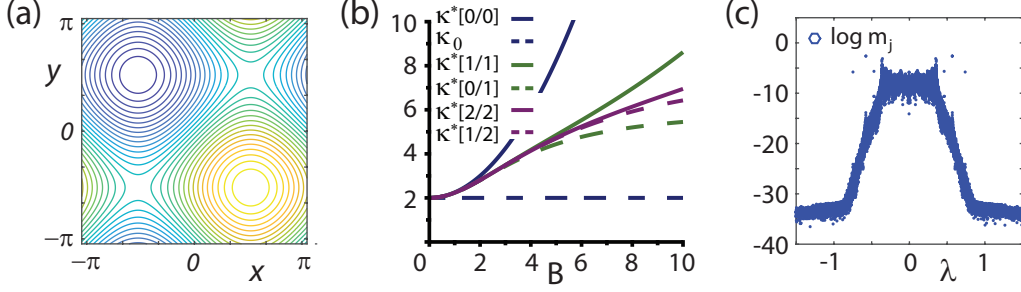


Figure 4: **Spectral behavior of effective diffusivities** (a) Streamlines for BC-flow with velocity field $v = (C \cos y, B \cos x)$ and $B = C = 1$. (b) Padé approximant upper $\kappa^*[M/M]$ and lower $\kappa^*[M - 1/M]$ bounds for κ^* , for various values of M , calculated via equation (14) for BC-flow with $C = B$, as a function of the flow strength B . (c) The spectral function (spectral masses m_j versus eigenvalues λ_j) computed via analogues of equations (7) and (8) [86].

perature \bar{T} and a symmetric, constant [91] effective conductivity tensor κ^* [110],

$$\partial_t \bar{T}(t, x) = \nabla \cdot [\kappa^* \nabla \bar{T}(t, x)], \quad \bar{T}(0, x) = T_0(x). \quad (12)$$

For simplicity, we focus on a diagonal coefficient κ_{kk}^* , $k = 1, \dots, d$, of κ^* , set $\kappa^* = (\kappa^*)_{kk}$, and write the non-dimensional velocity field $v = (\phi \ell / \tau) u$ and sea ice thermal conductivity $\varepsilon = \kappa_0 \tau / (\ell^2 \rho c)$, where τ and ℓ are system time and length scales, then [73, 3, 86, 87]

$$\kappa^* = \varepsilon(1 + \langle |\nabla w_k|^2 \rangle), \quad \langle |\nabla w_k|^2 \rangle = \int_{-\infty}^{\infty} \frac{d\nu(\lambda)}{\varepsilon^2 + \lambda^2}, \quad (13)$$

where $\langle \cdot \rangle$ denotes averaging over the space-time period cell.

Remarkably, the vector field $E(t, x) = \nabla w_k(t, x) + e_k$ satisfies equation (2) for two-component composite materials, with $J = \sigma E$, $\sigma = \varepsilon I + S$, $S = (-\Delta)^{-1} \partial_t + H$, and σ plays the role of the medium's conductivity tensor [86, 87]. Here, $H(t, x)$ is the *stream matrix*, given in terms of the incompressible velocity field $v = \nabla \cdot H$ and satisfies $H^T = -H$ [3, 2]. When the flow is time-independent, $v = v(x)$, then $w_k = w_k(x)$ and $S = H$. Moreover $\kappa^* = \sigma^*$, with $\sigma^* = (\sigma^*)_{kk}$ given [87] in equation (3). The integral representation for κ^* in equation (13) follows from the resolvent formula $\nabla w_k = (\varepsilon I + \imath \Gamma S \Gamma)^{-1} [-\Gamma H e_k]$, an analogue of equation (5). The *self-adjoint* operator $\imath \Gamma S \Gamma$, where $\imath = \sqrt{-1}$, involves the same projection operator $\Gamma = -\nabla(-\Delta)^{-1} \nabla \cdot$ as the setting of two-component composites. Equation (13) shows that brine advection *enhances* the thermal conductivity of sea ice $\kappa^* \geq \varepsilon$.

We have recently extended [86] our numerical methods discussed in Section 1.2.2 to compute the spectral measure ν for spatially periodic flows, as shown in Fig. 4(c), as well as the associated effective thermal conductivity κ^* . We have also developed Fourier methods for computing the spectral measure ν for space-time periodic flows [87]. These computations show that the origin in the space of the spectral parameter λ for advection-diffusion plays the role of the spectral endpoints 0 and 1 for composite materials, with an increase in spectral mass giving rise to an advection-driven enhancement of effective diffusivity above the thermal conductivity of sea ice with no brine flux. This is a key example of how the behavior of the

spectral measure ν governs the behavior of the bulk transport coefficient κ^* . We propose to employ these numerical methods to explore the properties of enhanced thermal conductivity in sea ice, exploring realistic velocity fields under various circumstances and how they impact thermal exchange processes, and extend our results to 3D flows such as the ABC-flow [13].

Analytical calculations of the spectral measure ν are extremely difficult except for simple flows like shear flow [3]. However, Padé approximants $[L/M]$ provide rigorous, converging upper and lower bounds [5] for the *Stieltjes function* $f(z) = \langle |\nabla w_k|^2 \rangle / z$ in equation (13), with $z = \varepsilon^{-2}$, using the moments ν_n of ν ,

$$[M - 1/M] \leq f(z) \leq [M/M], \quad f(z) = \sum_{n=0}^{\infty} (-1)^n \nu_{2n} z^n, \quad (14)$$

where the summation follows from writing $1/(1 + z\lambda^2)$ as a geometric series. Bounds for κ^* can also be obtained using variational methods [3, 34]. While the mathematical framework summarized by equations (12)–(14) provides an elegant, analytic representation for κ^* and a means to obtain tight bounds on κ^* , the lack of a method to calculate the moments ν_n of ν has impeded progress on obtaining explicit bounds for specific flows using this bounding procedure [3, 2] since 1991!

We have recently developed a mathematical framework [87, 86] that can be used to compute, in principle, *all* of the moments ν_n associated with a spatially or space-time periodic brine velocity field v , hence Padé approximant bounds, as shown in Fig. 4(b). This framework is equivalent to that described above, reproducing the result in (13) with the same measure ν [87, 86]. Instead of focusing on the vector field ∇w_k , the scalar field w_k is used, which has the resolvent formula $w_k = (\epsilon + G)^{-1}[(-\Delta)^{-1}v_k]$, $G = \iota(-\Delta)^{-1}D_t$ is a self-adjoint operator, v_k is the k th component of v , $D_t = \partial_t + v \cdot \nabla$ for time-dependent v and $D_t = v \cdot \nabla$ for time-independent v . Using this approach, the moments ν_n of ν , hence the bounds in equation (14) can be calculated exactly *in closed form*. Our recent results for BC-flow, with $v = (C \cos y, B \cos x)$ and $B = C$ are displayed in Figure 4.

We propose to further develop and investigate rigorous bounds on the convection enhanced thermal conductivity of sea ice with brine velocity fields. Field measurements of this key parameter are notoriously difficult, and there is very little theoretical work in this direction. We will also further develop this framework and apply it to a broad range of 2D and 3D steady periodic flows, as well as 2D and 3D space-time periodic flows. We also propose to develop inverse bounds [74, 75, 23, 20, 24, 124, 14, 22, 28, 50], which incorporate measurements of the effective thermal conductivity of sea ice to potentially recover geometric and dynamic information about the underlying fluid velocity field.

1.3.3 Fluid permeability and the trapping constant

Pivotal to understanding key processes in the physics and biology of sea ice is its fluid permeability, \mathbf{k} . This parameter controls bulk flow and depends on the fluid volume fraction and microstructural characteristics. Moreover, sea ice permeability controls the evolution of melt ponds and the summer sea-ice albedo, a key parameter in climate modeling, as well as the transport of nutrients and enzymes through the pore matrix of sea ice [49].

While studies of \mathbf{k} for sea ice are sparse, rigorous bounds on \mathbf{k} in general have been derived directly on \mathbf{k} using variational principles [97], and via variational bounds on the

trapping constant γ [115, 114, 113], where

$$\mathbf{k} \leq \gamma^{-1} I, \quad (15)$$

with I the identity matrix. Equality is achieved for a certain class of microstructures. The trapping constant [114, 113] is defined in terms of a porous medium that consists of a pore region, in which diffusion takes place, and a solid region whose shared boundary with the pore space contains “traps” which can absorb the diffusing species via a surface reaction. For a reactant diffusing in this type of porous medium an average survival time $\tau \sim \gamma^{-1}$ before a diffusing particle gets absorbed at the boundary. The trapping constant arises in areas such as nuclear magnetic resonance imaging [100, 33] or enzymatic bacterial foraging in porous sea ice or the sea floor [117].

We propose here a new method – the first to not rely on variational principles – for obtaining bounds on the trapping constant, which will yield bounds on the fluid permeability. We manipulate the trapping constant formulation and develop it into an analytic continuation method for obtaining rigorous bounds, in terms of the average of Green’s function over the pore space. We find a Stieltjes integral representation for the trapping constant which separates the component parameters from the geometry of the composite.

To consider the trapping problem, we let $\Omega = \Omega_p \cup \Omega_s$, where Ω_p and Ω_s represent the pore space and solid regions, respectively, $\Omega_p \cap \Omega_s = \emptyset$, and let $\partial\Omega_p$ denote the interface between the two regions. It was rigorously shown [113] that for statistically homogeneous isotropic media, $\gamma^{-1} = \langle u \rangle$, where $\langle \cdot \rangle$ denote the ensemble average, and u is a concentration field that satisfies

$$\begin{cases} \Delta u = -1, & \text{in } \Omega_p, \\ u = 0, & \text{on } \partial\Omega_p, \\ u = 0, & \text{in } \Omega_s. \end{cases} \quad (16)$$

To obtain a Stieltjes integral representation for the trapping constant γ , we consider a relaxed version of the trapping problem: let D be the local diffusion constant, with

$$D = \begin{cases} D_P > 0, & \text{on } \Omega_p, \\ D_S > 0, & \text{on } \Omega_s, \end{cases} \quad (17)$$

instead of $D_S = 0$, where u satisfies

$$\begin{cases} \nabla \cdot (D \nabla u) = -1, & x \in \Omega_p, \\ D \frac{\partial u}{\partial n} + \zeta u = 0, & x \in \partial\Omega_p, \\ \nabla \cdot (D \nabla u) = 0, & x \in \Omega_s, \end{cases} \quad (18)$$

where $0 < \zeta < \infty$ is a positive surface rate constant. If the solid phase, Ω_s , is a connected domain, we can recover the boundary condition in the limit as $D_S \rightarrow 0$.

Introducing the operator $A = \Delta^{-1} \nabla \cdot \chi_p \nabla$, we obtain an expression for u of the form

$$u = s(sI - A)^{-1}g, \quad s := \frac{1}{1 - D_S/D_P}, \quad g(x) = \frac{1}{D_P} \int_{\Omega_p} G(x - y) dy, \quad (19)$$

where g is the integral over the pore space of the Green's function, $G(x, y)$, corresponding to (18). Using the positive measure μ , corresponding to the spectral resolution of the operator A , we have derived a Stieltjes integral representation

$$\gamma^{-1} = \int_0^1 \frac{s d\mu}{s - \lambda}, \quad (20)$$

and obtained algebraic bounds of the form

$$\frac{\langle g \rangle + s - 1}{\langle g \rangle} \leq \gamma \leq \frac{s}{\langle g \rangle}. \quad (21)$$

Our main goal is to investigate this Stieltjes integral representation, the moments of the measure, and to obtain a sequence of bounds on the fluid permeability, through its relations to the trapping constant. An intermediate goal is to obtain explicit expressions of the bounds on the trapping constant in the 2-dimensional coated cylinder and 3-dimensional coated sphere models.

1.3.4 Complex viscoelasticity for wave propagation in the marginal ice zone

Striking correlations between Antarctic sea ice extent and wave activity have been found recently [62]. In both the Arctic and Antarctic, the ice floe size distribution in the marginal ice zone (MIZ) plays a central role in the properties of wave propagation though it. Ocean waves break up and shape the ice floes which, in turn, attenuate various wave characteristics. This ice-ocean interaction has become increasingly important in the Arctic, due to the dramatic decrease of the summer ice extent which is correlated with an increase in the size of the Arctic MIZ [109].

The MIZ can be thought of as a two component composite layer of ice and slushy water atop an inviscid ocean. Continuum models have been developed which describe wave propagation through the MIZ. However, the two component ice-slush composite microstructure of the layer is neglected in these models, and is instead described by a homogeneous layer that is purely elastic [7], purely viscous [60], or viscoelastic [119, 83] (the viscoelastic case generalizes the viscous and elastic cases). The effective elasticity, viscosity, and complex viscoelasticity, which describe the wave/ice interactions in these models, are difficult to determine. To help overcome this limitation, we have adapted the analytic continuation method for describing the transport of electromagnetic waves in two-component composite materials, discussed in Section 1.2.2, to provide an integral representation for the complex viscoelasticity [119], which explicitly incorporates the two-component ice-slush composite microstructure of the layer. This integral representation yields rigorous bounds on the effective complex viscoelasticity which depend on the geometry of the ice-slush composite and the complex viscoelasticities of the ice and slush phases.

We now review this mathematical framework. The ice-slush layer is thought of as a Kelvin-Voight material and modeled by a spring and dashpot. The deviatoric part of the stress tensor is given by $\boldsymbol{\sigma} = 2(G + \rho\nu \partial_t)\boldsymbol{\epsilon}$. Here G is the shear modulus, ρ is the density, ν the kinematic viscosity, $\boldsymbol{\sigma}$ is the stress tensor, and $\boldsymbol{\epsilon}$ is the strain tensor. The material is assumed to be linear and obey Hooke's law $\boldsymbol{\sigma} = \mathbf{C} : \boldsymbol{\epsilon}$, where \mathbf{C} is the elasticity tensor, $\boldsymbol{\epsilon} = \nabla^s u$, ∇^s

is the symmetric gradient, and u the displacement. If we consider a simple harmonic wave of frequency ω , then $\partial_t \epsilon = -i\omega \epsilon$, and we may write the deviatoric part of σ as $\sigma = 2\nu \epsilon$, where $\nu = G - i\rho\omega v$. Motivated by [22], we take $\mathbf{C} = \nu \mathbf{\Lambda}_s$, where $\mathbf{\Lambda}_s = \delta_{ik}\delta_{jl} + \delta_{il}\delta_{jk} - \frac{2}{3}\delta_{ij}\delta_{kl}$. Then we have that $\sigma = \mathbf{C} : \epsilon = 2\nu \epsilon$ (here $:$ is a contraction) since we assume our material is incompressible and therefore $\nabla \cdot u = 0$, which implies $\mathbf{\Lambda}_s : \epsilon = 2\epsilon$. We may also define the compliance tensor as $\mathbf{L} = \mathbf{C}^{-1}$, in this case we have $\epsilon = \mathbf{L} : \sigma$ where $\mathbf{L} = \nu^{-1} \mathbf{\Lambda}_s$. We will also take our material to be irrotational, $\nabla \times \epsilon = 0$. The momentum balance equation for the displacement can be stated as,

$$\nabla \cdot (\sigma + P\mathbf{I}) - \rho g e_z = \rho \partial_t^2 u. \quad (22)$$

In the long wavelength, low frequency limit $\nabla \cdot P\mathbf{I} \approx \rho g e_z$ and for harmonic waves $\partial_t^2 u = -\omega^2 u$. In this limit, we can drop terms of order ω^2 and simplify (22) with our pressure approximation, we obtain the quasi-static equation of motion $\nabla \cdot \sigma = 0$. These considerations lead to the system of equations,

$$\nabla \cdot \sigma = 0 \quad \mathbf{C} : \epsilon = 2\nu \epsilon = \sigma \quad (23)$$

$$\nabla \times \epsilon = 0 \quad \mathbf{L} : \sigma = \frac{1}{2\nu} \sigma = \epsilon. \quad (24)$$

Consider again our constitutive relation, $\sigma(x, \alpha) = \mathbf{C}(x, \alpha) : \epsilon(x, \alpha)$, (involving stationary random fields) where $x \in \mathbb{R}^d$, $\alpha \in \Omega$ where Ω is the set of all realizations of the random elastic medium. Since the ice-slush layer is a two-component composite material, we can write $\mathbf{C}(x) = (\mathbf{C}_1 \chi_1 + \mathbf{C}_2 \chi_2)$ Here $\mathbf{C}_i = \nu_i \mathbf{\Lambda}_s$ for $i = 1, 2$.

The effective elasticity tensor is defined to be the constant tensor which relates the average stress to the average strain $\langle \sigma \rangle = \mathbf{C}^* : \langle \epsilon \rangle$. In this particular case we require $\mathbf{C}^* = \nu^* \mathbf{\Lambda}_s$, this allows us to obtain bounds for the effective complex viscoelasticity ν^* . The key to obtaining the bounds is deriving an integral representation for ν^* involving a positive measure μ on the interval $[0, 1]$. In this case it is given by,

$$F(s) = 1 - \frac{\nu^*}{\nu_2} = \int_0^1 \frac{d\mu(\lambda)}{s - \lambda}, \quad s = \frac{1}{1 - \nu_1/\nu_2}. \quad (25)$$

Analogous to the two component composite setting discussed above, the integral representation in (25) follows from a resolvent formula for the strain,

$$\chi_1 \epsilon = s (s\mathbf{I} - \chi_1 \Gamma^s \chi_1)^{-1} \chi_1 \epsilon^0, \quad (26)$$

where $\epsilon^0 = \langle \epsilon \rangle$, $\Gamma^s = \nabla^s (\nabla \cdot \nabla^s)^{-1} \nabla \cdot$, and $\chi_1 \Gamma^s \chi_1$ is self-adjoint on an appropriate Hilbert space.

Information about the ice-slush geometry is encoded in the moments μ_n of the measure μ , which are given by equation (6) with $G = \chi_1 \Gamma^s \chi_1$. The mass of the measure is $\mu^0 = p_1$, the volume fraction of component 1. This, combined with an analogous integral representation for σ , allow us to derive bounds for the effective viscoelasticity ν^* . The bounds are derived by varying over the set of positive measures on $[0, 1]$ which are consistent with a given geometry. In the case that only the mass of the measure is known, the extreme points of the set of measures consistent with a prescribed fixed volume fraction are the one point measures

$p_1\delta_\lambda$. With this information we can determine that the effective parameter must lie between two circular arcs [85, 41].

The bounds are presented in Figure 5. At present only the mass of the measure is known, and due to the high contrast in the real part of the complex viscoelasticities of each component, 6-8 orders of magnitude, the bounds are very large. However, if more moments can be calculated tighter bounds can be obtained. The determination of higher moments can be difficult, assumptions about the geometry often simplify the calculations, such as assumptions of isotropy or a specific strain field. Assumptions about geometry can also lead to a restriction of the support of the measure μ , further tightening any known bounds.

Here we propose to significantly tighten these first bounds on the complex viscoelasticity of the sea ice pack by treating it as a *matrix-particle composite*, which yields a spectral gap and much tighter bounds. In previous work on the effective real valued conductivity of strongly heterogeneous composites [17], it was shown that for a composite composed of high contrast materials, in which one phase consists of non-touching grains embedded in a matrix of the other material, the support of the measure μ in the analogous integral representation of (25) for the effective conductivity, may be restricted. This has the effect of dramatically tightening the bounds of the effective parameter. In [44] this idea was extended to the complex case and applied to the electrical permittivity of sea ice. In 2-d we may consider the inclusions to be disks of radius r_{inc} surrounded by a “corona” of matrix material with outer radius r_{mat} . In this case, the support of the measure is $[S_m, S_M]$ where,

$$S_m = \frac{1}{2}(1 - q^2), \quad S_M = \frac{1}{2}(1 + q^2) \quad (27)$$

and $q = r_{inc}/r_{mat}$ is the ratio of the radius of the inclusion to that of its corona of matrix material. Note that the further the separation of the inclusions, the smaller the support and when $q = 1$, the inclusions touch, and the support is $[0, 1]$.

The ice water composite geometry resembles that of a matrix-particle composite. That is, we may think of the ice phase as a set of non touching disks embedded in a matrix of viscous slush. This is especially true near the edge of the MIZ where immense areas of water are covered in disk shaped pancake ice. Given the similarities between the governing equations in the complex permittivity and the quasistatic complex viscoelasticity case, we expect the matrix-particle bounds to apply. Initial calculations suggest that the matrix-particle bounds do indeed apply to this situation and provide a very compact set of parameters, although further proof is required. Improvement of the bounds through higher moment calculation and derivation of a matrix particle bound will be the major focus of our work.

In the long wavelength, low frequency regime, many of the waves which propagate into the ice pack are effectively plane waves. In this case, we may model wave motion through the MIZ with a simple 1-d wave equation involving the effective viscoelasticity, $u_{xx} = (\rho/2\nu^*)u_{tt}$. In this situation, both the wave number and attenuation rate of a propagating wave are determined by the effective parameter as a function frequency. Since the geometry of the floes determines the effective viscoelasticity, this facilitates a simple propagation model which still takes into account all of the important properties of the floe geometry. This has potential use in improving current sea ice models by providing a simple, numerically inexpensive way to update the rheological properties and wave propagation characteristics of the model ice pack as it evolves. We have investigated the ability of such simple models to capture some

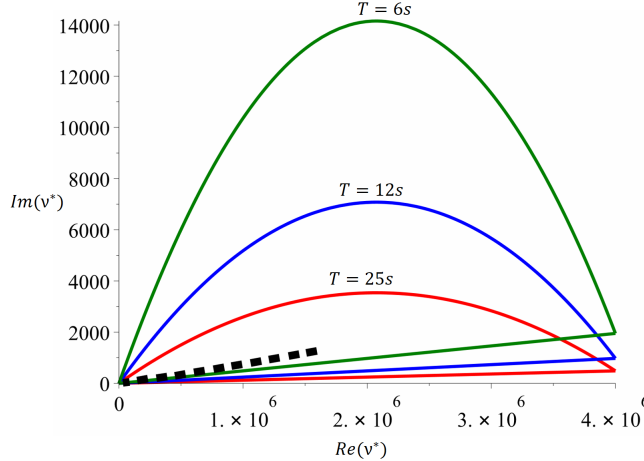


Figure 5: Bounds for $\bar{\nu}^*$ plotted for several periods, $T = 2\pi/\omega$, with $G = 10^7 Pa$, $\nu = 5$ for the ice phase and $G = 10 Pa$, $\nu = 14 \times 10^{-3}$ for the slush phase and $p_1 = 0.4$. We have plotted the complex conjugate of ν^* to better highlight the contrast in the parameters. The dotted line is data extracted from the work in [36, 76] for periods $6s \leq T \leq 25s$.

of the properties of the MIZ with some success. Using the effective parameter to define wave characteristics of waves propagating in the MIZ and following ice-wave breaking criteria in [32], we were able to capture some of the average properties of the MIZ, which were in good agreement with measurements of maximum floe sizes observed in [116].

1.4 Low order models and large scale advection diffusion

1.4.1 Advection diffusion in the marginal ice zone

Dense pack ice transitions to open ocean over a region of broken ice termed the marginal ice zone (MIZ) – a highly dynamic region where the ice cover lies close to an open ocean boundary and intense atmosphere-ice-ocean interactions take place [65]. The morphology of the MIZ is governed by coupled thermodynamic and dynamic processes including advection and diffusion. The width of the MIZ is a fundamental length scale for polar dynamics [118] in part because it represents the distance over which ocean waves and swell penetrate into the sea ice cover. Moreover, MIZ width is an important spatial dimension of the marine polar habitat, and impacts human accessibility to high latitudes [96]. We recently uncovered a dramatic 39% widening of the summer Arctic MIZ based on objective analysis of three decades of satellite-derived sea ice concentrations [109]. Here we will investigate the role of diffusivity in MIZ morphology. We will use cutting edge observational and modeling strategies that span a range of scales from short-term floe-scale behavior to seasonal-to-decadal cycles and trends at the scale of the MIZ.

Our MIZ-scale investigation of diffusivity is motivated by our prior work using Laplace’s equation to study MIZ shape and morphology, and in particular the deviation of MIZ concentrations from the solution of Laplace’s equation. The MIZ is in general not geodesically convex, as illustrated by the example in Fig. 6. Sea ice concentration $c(x, y)$ is used here to define the MIZ as a body of marginal ice ($0.15 \leq c \leq 0.80$) adjoining both pack ice

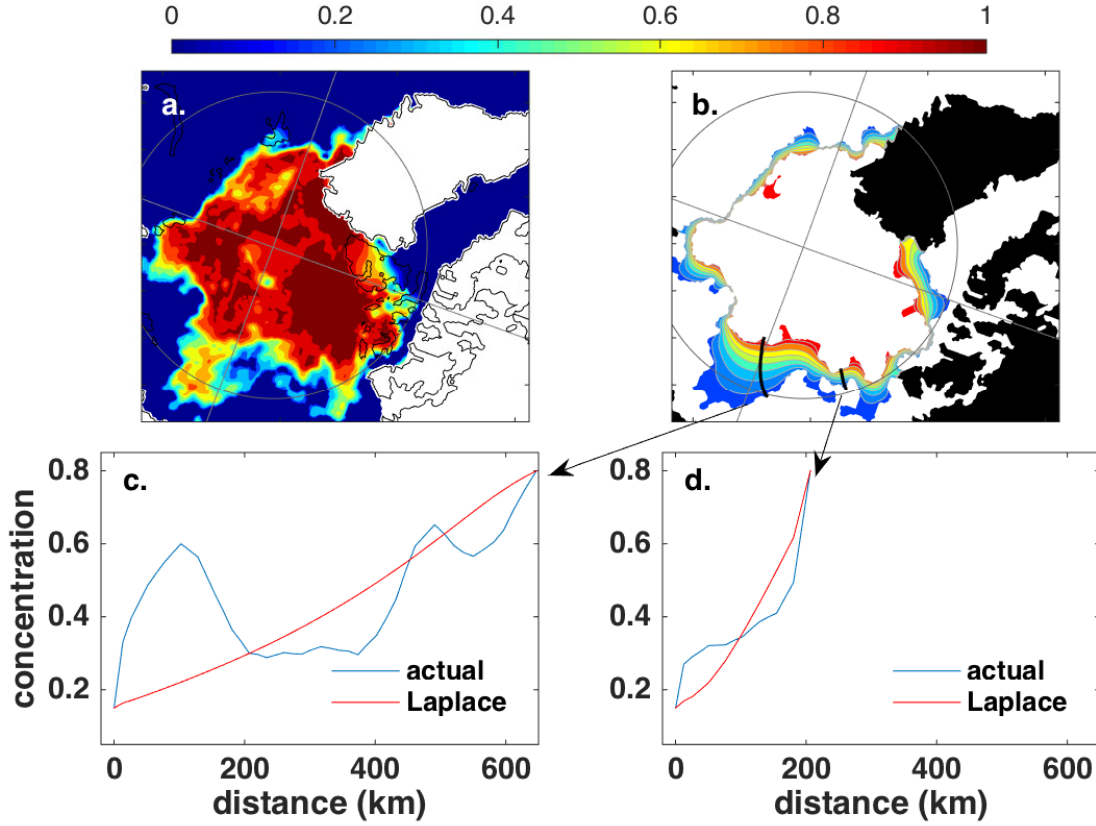


Figure 6: For 29 August 2010: (a) passive microwave sea ice concentrations (shading), (b) solution to Laplace’s equation within the marginal ice zone (shading), and (c,d) observed concentration (blue) and solution to Laplace’s equation (red) along two streamlines indicated by black curves in panel (b).

($c > 0.80$) and sparse ice ($c < 0.15$). To define an objective MIZ width applicable to such shapes, Strong [105] introduced the idea of an idealized sea ice concentration field $\psi(x, y)$ satisfying Laplace’s equation within the MIZ

$$\nabla^2 \psi = 0. \quad (28)$$

We use (x, y) here to denote a point in two dimensional space, it is understood that we are working on the spherical Earth, and solutions can be obtained in the data’s native stereographic projection because solutions of Laplace’s equation are invariant under conformal mapping [102]. The solution to (28) for the example in Fig. 6a is shown by color shading in Fig. 6b. Any curve γ orthogonal to the level curves of ψ and connecting two points on the MIZ perimeter (a field line through the gradient field $\nabla \psi$; black curves, Fig. 6b) is contained in the MIZ, and its length provides an objective measure of MIZ width (ℓ). Analogous applications of Laplace’s equation have been introduced in medical imaging to measure the width or thickness of human organs, and we have detailed desirable mathematical properties

of this method including invariance with respect to translation and rotation on the sphere, uniqueness at every point in the MIZ, and generality including applicability to non-convex shapes [106]. Building on the advances above, we propose a more general form of (28),

$$\nabla \cdot (\sigma \nabla \psi) = 0, \quad (29)$$

which is a natural generalization, both mathematically and physically, as equation (29) can be viewed as a steady state version of the effective diffusion equation (12) that is obtained by homogenizing the advection diffusion (11). Hence, the function ψ is an approximation of $\bar{\phi}$ which solves the effective diffusion equation (12) when temporal variations in the ice cover concentrations are neglected. The introduction of a local conductivity field $\sigma = \sigma(x, y)$ or a local diffusivity field $D = D(x, y)$ will enable the idealized sea ice concentration field ψ to faithfully reflect sea ice rheology and variability, with fluctuations in $\psi(x, y)$ related to the inhomogeneities in σ or D . In particular, in the electrical analogue, $E = -\nabla \psi$ plays the role of an electric field, with $J = \sigma E$ an electric current density, as in classical electrodynamics, where ψ is thought of as an electric potential.

We will also address the development of a time dependent PDE model for the concentration $\psi(x, y, t)$. The natural way of introducing time dependence is through $\partial \psi / \partial t = \nabla \cdot (D \nabla \psi)$. However, this equation is limited in that it does not allow for advection of the concentration field through atmospheric, oceanic and thermodynamic forcing. As a first step in this direction, we will consider the equation

$$\frac{\partial \psi}{\partial t} = \nabla \cdot (D \nabla \psi) - \nabla \cdot (\psi v), \quad (30)$$

where the vector field v represents an effective concentration advection by wind and ocean currents, and potentially also thermodynamically driven changes in concentration related to atmospheric and oceanic heat flux.

1.4.2 Inversion of the concentration field for spatially varying diffusivity

Consider an actual satellite-derived concentration field $\psi(x, y)$ satisfying (29) with boundary conditions $\psi = 0.15$ where MIZ borders a sparse ice region and $\psi = 0.80$ where the MIZ borders a pack ice region. Reconstruction of $\sigma(x, y)$ from observations of the concentration field $\psi(x, y)$ in (29), is an *inverse problem*. Because of its more general form, the idealized sea ice concentration field given by (29) will more closely correspond to the observed sea ice field than did the solution from (28). For an isotropic conductivity or diffusivity function $\sigma(x, y)$ consider the steady state diffusion equation:

$$\nabla \cdot \sigma \nabla w = 0 \quad \text{in } \Omega, \quad w = \psi \quad \text{in } \Omega, \quad (31)$$

where Ω is the region of Earth's surface of interest. To find the diffusivity σ , we propose to solve the following constrained minimization problem:

$$\min_{\sigma} \|w - \psi\|_{L^2(\Omega)}^2 \quad \text{subject to} \quad \nabla \cdot \sigma \nabla w = 0 \quad \text{in } \Omega. \quad (32)$$

As a simplified example, let us consider a one-dimensional steady-state problem. In Fig. 6c and 6d, the one-dimensional profiles of observed ice concentration (blue) are shown along

two streamlines indicated by black curves in panel (b). In this 1D problem, the diffusivity could be estimated as a reciprocal of the gradient of the concentration function. However, instability of this solution indicates the ill-posedness of the problem, which requires regularization to formulate a well-posed problem. We have noticed that the variations in the concentration function correspond to the particular behavior of the underlying oceanic flow.

Observe that in the steady state equation (31), we assumed that the right hand side of the equation $\nabla \cdot (D\nabla\psi) = \partial\psi/\partial t$ is small and can be neglected. This corresponds to slow time variations in the geometry of the ice field. However, the proposed method should work for a more general case when this assumption is dropped. We plan to investigate the inverse problem of reconstruction of the diffusivity for a general diffusion equation which corresponds to the effective large scale, long time behavior of advection diffusion. The reconstructed diffusivity coefficient will characterize the dynamics and spatio-temporal characteristics of the fluid flows of the underlying advection-diffusion.

As we show in [87], homogenization of the advection-diffusion equation results in the effective diffusion equation with the enhanced effective diffusivity D^* which characterizes the effective transport by fluid velocity fields. The information about the velocity field is contained in the spectral measure μ in the Stieltjes integral representation of the effective diffusivity D^* . In previous work, we developed methods for solving the inverse homogenization problem [20, 22, 23] to recover microstructural information from the measured effective electrical or viscoelastic properties of the composite, or from observations of the effective properties of the medium, such as the effective conductivity σ^* associated with $\sigma(x, y)$. The approach is based on reconstruction of the spectral measure μ or its moments from the measurements of the effective parameters of the composite. We plan to extend this approach to the problem discussed here. Reconstruction of the conductivity σ and comparison with variations in the concentration field, as well as with oceanic, atmospheric, and thermodynamic forcing will give valuable insights into the components of sea ice physics which are acting to influence ψ and the PDE's modeling its evolution. Solving this inverse homogenization problem will allow us to recover subscale information about the oceanic and atmospheric flows.

1.4.3 Filling the polar data gap

Our team recently used Laplace's equation as a foundation for objectively *filling the polar data gaps* where satellite orbits do not provide observations (Fig. 7). For many years it was assumed that this northernmost region of the Arctic was always covered with sea ice. However, recent precipitous losses in the polar ice pack call into question this assumption, which can significantly affect overall estimates of Arctic sea ice volume, for example. Such dramatic changes motivate development of an *objective* method for estimating unobserved concentrations within the gap.

We proposed [107] a partial differential equation-based model with tuned stochastic spatial heterogeneity to estimate the concentrations within a region Ω on Earth's surface,

$$f(\theta, \phi) = \psi(\theta, \phi) + W(\theta, \phi),$$

where θ is longitude and ϕ is latitude, or $f(r) = \psi(r) + W(r)$ where $r \in \Omega$. We suggested prescribing the scalar field ψ to be a solution of Laplace's equation (28) in spherical co-

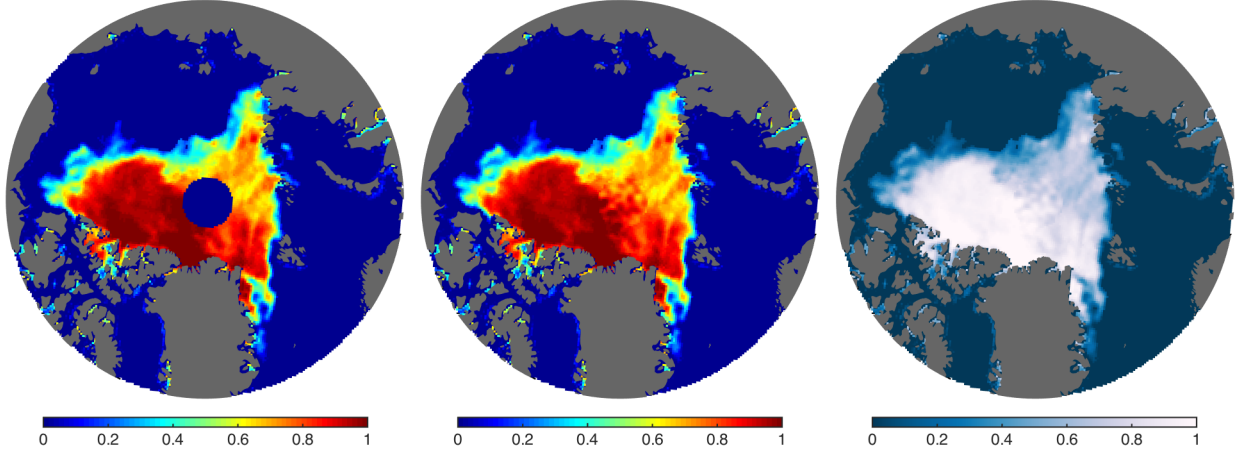


Figure 7: The left image is an example of the polar data gap (dark blue disc) on 30 August 2007 with shading outside the disc indicating concentration. The middle and right images show the data fill presented here, with the color shading at right similar to that used by the National Snow and Ice Data Center (<http://nsidc.org>).

ordinates with boundary conditions taken from observations on the boundary of the polar data gap $\partial\Omega$. If $\partial\Omega$ is sufficiently smooth and the concentration is a continuous function along $\partial\Omega$, a unique solution for ψ exists, and can be obtained numerically by expressing the Laplacian as a second-order finite difference operator. The stochastic term W provides realistic deviations from ψ , and was tuned by collecting samples W_s of the difference between observed concentrations and ψ in three circular regions C_j , $j = 1, 2, 3$, around the polar data gap

$$W_s(r) = f_{\text{obs}}(r) - \psi(r), \quad r \in C_j, \quad j = 1, 2, 3,$$

where f_{obs} denotes observed concentrations. Based on analysis of thousands of samples, we formulated a seasonally varying amplitude for W and introduced realistic spatial autocorrelation by convolution of spatially uncorrelated noise with a Gaussian function. Figure 7 shows an example of this model applied to the polar data gap for 30 August 2007. Tests in regions around the polar data gap showed observation-model correlations of 0.6 to 0.7 and absolute deviations of order 10^{-2} or smaller.

We plan to extend this research using several related approaches. First, we will draw on more detailed formulations for sea ice concentration based on spatially varying diffusivity, leveraging insights we gain from mathematical investigation described above in Section 1.4.2. Second, we will extend the gap filling formulation to investigate the case of spatial variations in diffusivity and spatial and temporal variations in concentration, $\nabla \cdot (\sigma \nabla \psi) = \partial \psi / \partial t$. To model the stochastic term W and temporal variations of the concentration function, we will use the Wiener (polynomial) chaos expansion method. Finally, we will formulate the data gap fill as a Cauchy problem. In this approach, we will use the concentration data in surrounding areas to assign Dirichlet and Neumann conditions on the boundary $\partial\Omega$, meaning we begin with observations of concentration ψ and $\partial \psi / \partial n$ on $\partial\Omega$, where n is normal to $\partial\Omega$. The Cauchy problem is well known to be a highly ill-posed problem whose solution does not continuously depend on the boundary data. For such a problem, small errors in the

given boundary data may result in very large errors in the numerical solution. The ill-posed Cauchy problem can be solved with appropriate regularization techniques drawing on our team’s related expertise. We plan to investigate various regularization methods that will analyze available concentration data in the surroundings to impose constraints on the solution and ensure well-posedness of the problem and stability of the numerical calculations.

1.4.4 Anomalous diffusion in the marginal ice zone

Understanding the long time, large scale transport of sea ice by atmospheric and oceanic flows is essential to an understanding of how ice pack characteristics evolve. In recent work [66], buoys were placed on sea ice floes and the subsequent dynamics were analyzed using Lagrangian dispersion statistics. This led to the striking discovery that the dynamical behavior of ice floes can be described in terms of anomalous diffusion. In particular, the dispersion of the buoys was measured in terms of the absolute mean-squared-displacement $A^2 = \langle |x_k(t) - x_k(0) - \langle x_k(t) - x_k(0) \rangle|^2 \rangle$ of the location x_k of the k^{th} buoy relative to its starting position, where $\langle \cdot \rangle$ denotes ensemble averaging of the positions of appropriate groups of buoys as a function of time t [67]. The long time temporal scaling $A^2 \sim t^\alpha$ of the dispersion is described by the Hurst exponent α , which is a measure of autocorrelation and long-time memory of the time series [71].

Diffusive behavior ($\alpha = 1$) of the buoys was observed in the marginal ice zone (MIZ), implying that the floe trajectories resemble Brownian motion [67]. In coherent flow structures, such as the transpolar drift stream and the Beaufort Gyre, the ice dynamics exhibit super-diffusive behavior ($\alpha > 1$) [67]. This regime captures long-range correlations and organized structure in the flow field, with ballistic ($\alpha = 2$), elliptic ($\alpha = 5/3$), and hyperbolic ($\alpha = 5/4$) regimes providing signatures of advection, vorticity-dominated, and shear-dominated flow, respectively [67]. In more crowded, thicker ice covers, floe-floe interactions suppress kinetic energy, giving rise to trapping phenomena and sub-diffusive behavior ($\alpha < 1$) [67]. The magnitude of the sub-diffusive scaling was shown to correspond spatially with patterns, characterized by deformation [95, 67], in sea ice concentration and thickness.

We have been developing a framework to model the long time, large scale transport of sea ice and the observed dynamics. Thus far, our simulations model ice floes as disks confined to a plane and experiencing forces, $F = ma$ where m is the mass of the particle and a is acceleration, from flow-particle interactions and particle-particle collisions. Fig. 8 shows numerically simulated stages of vortex formation in the particle flow which mimic a gyre structure. *Verlet-velocity Integration* was used to approximate disk motion [54]. After experimenting with several types of interactions [70, 54], we found that viscous drag and spring-dashpot collisions best mimicked the behavior and statistical properties of observed ice floes within a broad parameter range. Physically relevant mechanics such as ridging and rafting, melting, variable drag and ice floe size can be implemented by varying interactions and simulation parameters.

As discussed above (see also [91, 94, 87]), we can reduce the analysis of scalar transport by complex velocity fields v to solving effective or *homogenized* equations. Homogenization of the advection-diffusion equation for the concentration, ϕ , with local diffusivity D , yields a diffusion equation involving an effective diffusivity tensor D^* . Integral representations for D^* encode the complex geometry and flow characteristics of the system via the *spectral*

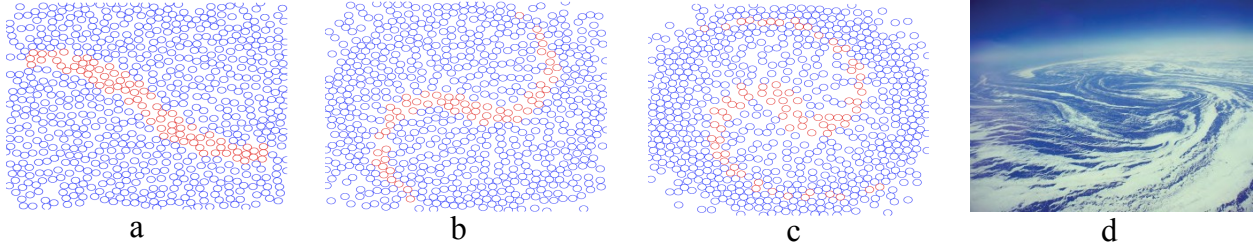


Figure 8: Numerically simulated sea ice floe patterns (a-c) which mimic formation of vortex structures such as in (d).

measure of a self-adjoint operator [91, 87]. We plan to find effective equations that include mechanical redistribution and melting to extend our analysis to these phenomena.

Anomalous diffusion of constitutive particles in physical systems which exhibit sea ice-like dynamics has been modeled by *continuous time random walks* [94]. In this approach, we consider probabilistic motion dX of a tracer, such as $dX = vdt + dW$, where dX and dW are random variables and vdt is determined from flow fields. From data, the behavior of dW can be inferred from particle-particle interactions by robust estimation methods. Using *stochastic calculus* [94], an equation describing the concentration of particles ϕ is

$$\frac{d\phi}{dt} = D_t^{1-\alpha} \left[\Delta \frac{V'(x)}{m\eta_1} + \nabla K_\alpha \right] \phi(x, t),$$

where $D_t^{1-\alpha}$ is a *fractional differential operator* and m, η_1 , and K_α are computable constants. These equations are *fractional space-time diffusion equations* [94, 58] for which inverse methods can be applied to approximate parameters, notably advective terms and diffusion coefficients, from ϕ . To apply our work specifically to sea ice, we will use statistical methods to quantify the ranges of long scale, long time quantities such as α and deformation. Within these ranges our proposed framework can be used to understand experimental error and likely dynamical regimes. We are quite interested in the connection between Hurst exponents describing large scale floe dynamics and the characteristics of the ice pack.

The method can incorporate complicated ice floe interactions into a numerically homogenized model of forced motion of ice fields. With inclusion of modes of ice floe interaction such as ridging, rafting, collisions with variable drag, freezing and melting, we anticipate that the resulting effective behavior will be described by *fractional space-time diffusion equations*. We will use this new numerical model to solve the small scale cell problem for a realistic sea ice field, noting that this solution is needed to calculate coefficients of the homogenized problem. This numerical homogenization will extend the technique to realistic features of sea ice fields in the MIZ.

1.5 Statistical physics of melt pond evolution

The albedo of melting Arctic sea ice, a key parameter in climate modeling, is primarily controlled by surface melt ponds [93]. As melt ponds form and evolve, their connectivity impacts horizontal melt water transport, facilitates drainage through macro-pores such as seal

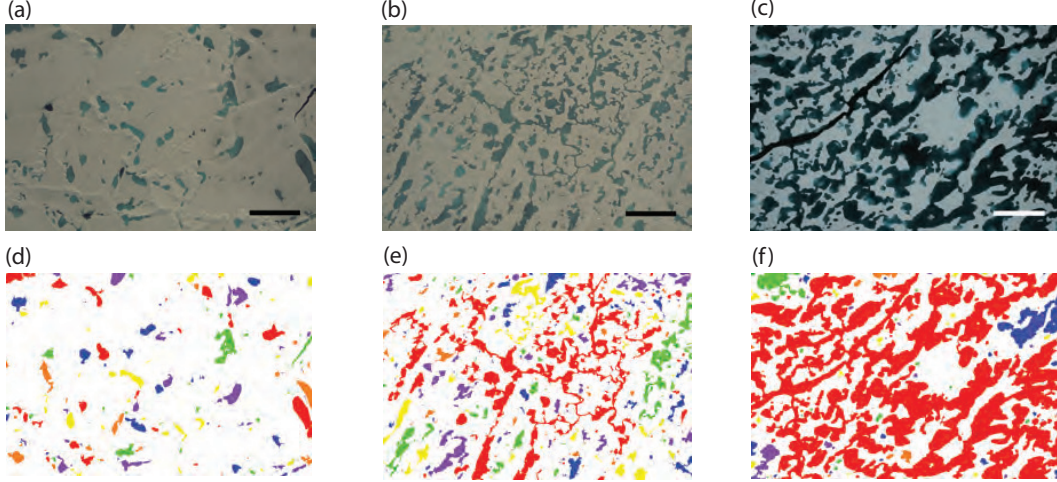


Figure 9: Evolution of melt pond connectivity. (a) Disconnected ponds, (b) transitional ponds, (c) fully connected melt ponds. The bottom row shows the color coded connected components for the corresponding image above: (d) no single color spans the image, (e) the red phase just spans the image, (f) the connected red phase dominates the image. The scale bars represent 200 m for (a) and (b), and 35 m for (c).

holes, cracks, and leads, and promotes floe breakage and fracture. A critical parameter to be investigated is the pond area fraction that constitutes the percolation threshold, meaning the pond coverage for which large scale connectivity emerges. How is the recently discovered transition in fractal geometry of melt ponds around a critical area of approximately 100 m^2 [56] related to triggering of percolation? How are melt pond connectivity and pond size distribution [92] impacted by initial cryospheric topography and ensuing sea ice albedo feedback during the melt season? Leveraging our recent advances, we will investigate these questions using melt pond models based on stochastic surfaces, a thermodynamically-motivated Ising model, and a physically-based partial differential equation model that incorporates melt rates and horizontal transport through porous media.

1.5.1 Percolation theory for melt ponds

We have developed a stochastic surface melt pond model in which we formulate the snow and ice topography using a two dimensional Fourier series with random coefficients. In particular, we use a finite cosine expansion with phase given by independent identically distributed uniform random variables and amplitude coefficients given by the physical properties of an observationally-calibrated autoregressive relation. The melt water level is then simulated by raising a plane upward through the surface, with the volume between the surface and the plane representing melt ponds (e.g., Fig. 10, upper row). We have demonstrated that the stochastic surface model captures the transition in fractal dimension discovered for observed melt ponds [15].

Our new directions of investigation with the stochastic surface model reveal percolation behavior that resembles results for simple two-dimensional lattices. To illustrate, we consider a two-dimensional square lattice with $L \times L$ sites and occupation probability p . If the site at

position vector r_i is occupied, the site-site correlation function $g(r_i, r_j)$ gives the probability that a site at r_j is a member of the same cluster. The function g is assumed to decay with large distance $d = |r_i - r_j|$ according to

$$g(d) \sim \exp\left(-\frac{d}{\xi(p)}\right), \quad (33)$$

where $\xi(p)$ is referred to as the correlation length. Theory indicates that $\xi(p)$ should obey

$$\xi(p) \sim -\nu \ln(|p - p_c|), \quad p \rightarrow p_c^- \quad (34)$$

where $\nu = 4/3$ is the universal critical exponent in two dimensions and p_c is the percolation threshold. For the two-dimensional square lattice, the value $p_c = 0.59274621$ has been determined numerically [90]. Our preliminary analyses of melt ponds in satellite remote sensing imagery is limited by small sample size, but suggests that melt ponds have a percolation threshold which is significantly lower than the value for the two-dimensional square lattice. Detailed study of large ensembles of stochastic surface model results indicates a percolation threshold for melt ponds of $p_c = 0.492$ (Fig. 10a). Interestingly, the stochastic surface model nonetheless exhibits correlation length scale behavior consistent with the critical exponent $\nu = 4/3$ expected for the simpler case of lattice percolation. This intriguing result suggests that the spatial correlation structure of melt ponds is sufficiently short-range so that the system falls within a standard universality class [57], meaning powerful analytical results can be leveraged in developing novel methods for incorporating melt pond evolution into predictive sea ice models.

We will also investigate melt pond evolution with a model that alters the sea ice topography via melting and uses partial differential equations to simulate horizontal transport [68]. The meltwater depth h evolves in the PDE model according to the equation

$$\frac{\partial h}{\partial t} = \text{He}(h) \left[-s + \frac{\rho_{\text{ice}}}{\rho_{\text{water}}} m - \nabla \cdot (hu) \right], \quad (35)$$

where the Heaviside step function

$$\text{He}(h) = \begin{cases} 1 & \text{if } h \geq 0, \\ 0 & \text{if } h < 0, \end{cases} \quad (36)$$

prevents h from becoming negative. The parameter $s = 0.8 \text{ cm day}^{-1}$ is the seepage rate, ρ is material density, g is gravitational acceleration, and the ice melt rate m increases linearly with melt pond depth. The horizontal velocity of melt pond water through porous sea ice is governed by Darcy's law

$$u = -\frac{g\rho_{\text{water}}}{\mu} \Pi_h \nabla \Psi, \quad (37)$$

where μ is the dynamic viscosity, Π_h is the fluid permeability, and $\Psi = z + h$ is the height of the surface Z at the location plus any overlying melt pond water depth at that location. Comparing the stochastic surface model to the more physically-based partial differential equation (PDE) melt pond model yielded results that were surprisingly similar overall, but

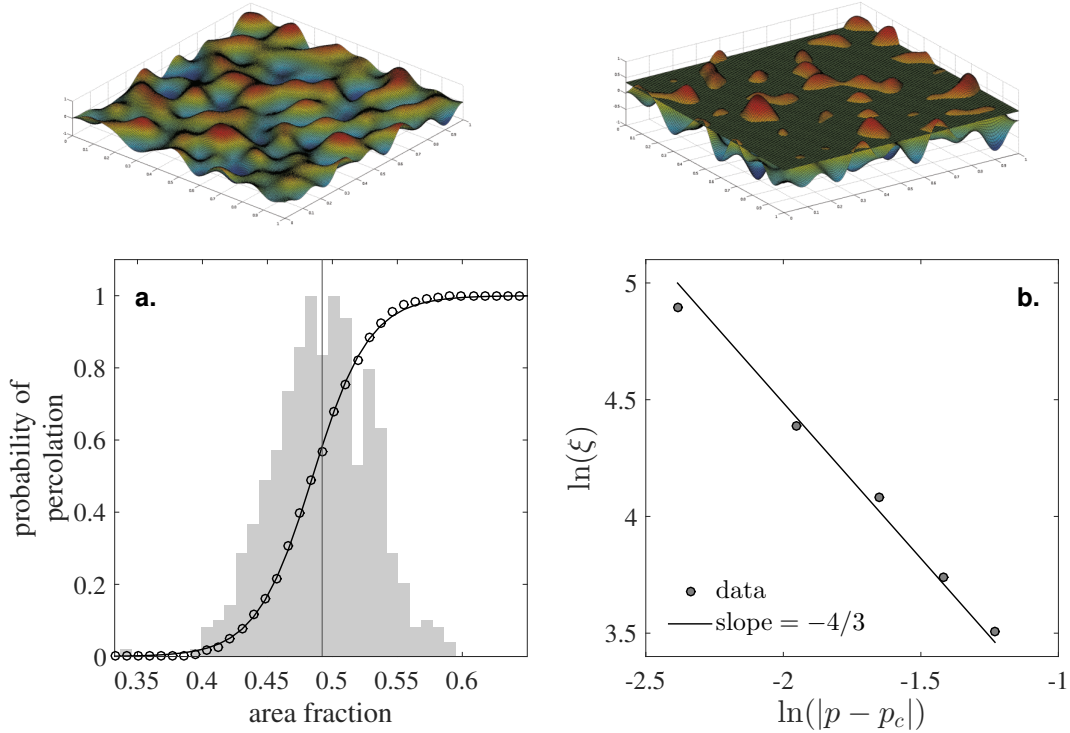


Figure 10: Upper row shows an example of the stochastic surface we developed for snow/ice topography (left) and the intersection of this surface with a plane representing the water level (right). (a) For the stochastic surface model, probability of percolation calculated within bins of area fraction (circles). The curve is a hyperbolic tangent fit, the shading is a normalized histogram of the area fraction at which percolation occurred for 500 realizations of the stochastic surface model, and the vertical dashed line indicates the percolation threshold $p_c = 0.492$. (b). Comparison of output from the stochastic surface model (filled circles) to the slope $-\nu = -4/3$ given by the universal exponent ν .

with some important contrasts. Specifically, we found that the limiting fractal dimension of the plane model is lower than the PDE model on average due to the tendency of the plane model to flood the surface. In comparison, the PDE model tends to melt downward into the surface and create complex pond shapes. For both models, we found that properties of the shift in fractal dimension, such as its amplitude, phase and rate, depend on the anisotropy and autocorrelation length scales of the topography.

We will continue analyzing arrays of remotely sensed melt pond imagery, and an important remaining unknown are the critical exponents that characterize melt pond evolution as large scale connectivity or percolation is approached. By replicating the evolution of observed melt pond percolation dynamics and fractal geometry with parsimonious mathematical models, we gain fundamental understanding of the underlying mechanisms and lay the foundation for enhancing the fidelity of numerical prediction frameworks currently lacking explicit representation of melt pond physics.

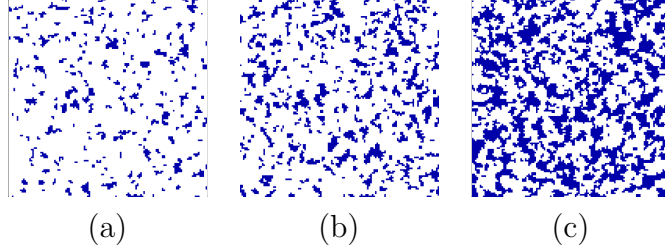


Figure 11: Illustrating results from the Ising model for melt pond evolution, the spin configurations s^i (blue is pond and white is ice) on a 128×128 portion of the lattice for three time periods: (a) shortly after the model begins with a random initial state, representing conditions early in the melt season, (b) approximately half way through the melt season with connected structures beginning to form, and (c) a mature simulated pond configuration representing conditions late in the melt season.

1.5.2 Ising model for melt ponds

Further insight into the dynamics of melt pond evolution is available by building on models arising from statistical mechanics. In particular, we have developed an Ising model which realistically simulates key properties and behavior of observed melt ponds. The general form of the Ising free energy can be written

$$\mathcal{H} = - \sum_i H^i s^i - \sum_{\langle i,j \rangle} J^{ij} s^i s^j, \quad (38)$$

where the index i ranges over a two-dimensional square lattice with periodic boundary conditions, and $\langle i, j \rangle$ denote nearest neighbors. The state variable is a binary (or spin) variable s^i such that $s^i = +1$ corresponds to water and $s^i = -1$ corresponds to ice. The term H^i is classically the external magnetic field, and we consider it as solar forcing for the melt pond application. The J^{ij} terms represent coupling constants.

To describe nontrivial spin clustering at zero temperature, the fields H^i and/or the bonds J^{ij} are chosen as random variables, and the resulting models are collectively known as disordered Ising models [88]. At zero temperature, the system is usually assumed to follow the Glauber single spin-flip dynamics [63]: at each update step, the attempted spin flip is accepted if \mathcal{H} decreases and rejected if \mathcal{H} increases. The system eventually converges to a local minimum of \mathcal{H} , known as a metastable state. Despite their importance, metastable states are not completely understood theoretically, with analytical results largely restricted to 1D [30] and many intricate issues remaining in 2D [89].

For melt ponds, the model is initialized with a pre-melt ice topography (h) assumed to be spatially independent Gaussian random variables with zero mean and unit variance. We specify the lattice constant $a = 0.85$ m as the threshold above which observed ice topography exceeds a null red noise spectrum. We consider a form of \mathcal{H} representing the total energy transfer between neighboring sites

$$\mathcal{H} = \sum_{\substack{\langle i,j \rangle: \\ s^i > 0, s^j < 0}} (\alpha_1(h^i) + J\alpha_2(h^j)), \quad (39)$$

where $J = 3.5$ is the ratio between the thermal conductivity of ice and water, α_1 is the water depth if the site becomes water, α_2 is the ice height if the site becomes ice, and W is a large negative constant that represents a reference water level far below the pre-melt ice topography. Here, the sum is taken only over the interfaces between water and ice, assuming that the energy transfer between two water sites or two ice sites is identically zero. The pond characteristics simulated by this model evolve from a purely random initial state into realistic pond configurations (e.g., Fig. 11) which replicate observed size distribution power law scaling and capture the observed transition in fractal geometry near the critical area of about 100 m^2 .

We will advance our Ising melt pond model by incorporating the effects of sea ice-albedo feedback. In the observed system, albedo decreases as ponds deepen, and the resulting increase in absorbed solar radiation tends to further deepen meltwater. One approach to capturing these effects in the model is to modify the interaction terms of the free energy \mathcal{H} to penalize flipping persistent water to ice, and also to penalize retaining ice adjacent to persistent water. In this way, locations which remain meltwater ($s^i = +1$) through many updates become more resistant to flipping to ice and are also more influential on the tendency for neighboring ice locations to flip to water. We will investigate whether further realism may be achieved by scaling the strength of the ice albedo feedback effects according to ice topography (h) and pond depth (α_1). Through these advances to this novel melt pond model, we retain the elegance of a simple statistical model for phase transitions while incorporating one of the most important positive feedbacks in the Arctic system.

1.6 References

- [1] S. A. Arcone, A. J. Gow, and S. McGrew. Structure and dielectric properties at 4.8 and 9.5 GHz of saline ice. *J. Geophys. Res.*, 91(C12):14281–14303, 1986.
- [2] M. Avellaneda and A. Majda. Stieltjes integral representation and effective diffusivity bounds for turbulent transport. *Phys. Rev. Lett.*, 62:753–755, 1989.
- [3] M. Avellaneda and A. Majda. An integral representation and bounds on the effective diffusivity in passive advection by laminar and turbulent flow. *Comm. Math. Phys.*, 138:339–391, 1991.
- [4] M. Avellaneda and M. Vergassola. Stieltjes integral representation of effective diffusivities in time-dependent flows. *Phys. Rev. E*, 52(3):3249–3251, 1995.
- [5] G. A. Baker and P. R. Graves-Morris. *Padé Approximants*. Encyclopedia of Mathematics and its Applications. Cambridge University Press, 1996.
- [6] S. Barabash and D. Stroud. Spectral representation for the effective macroscopic response of a polycrystal: application to third-order non-linear susceptibility. *J. Phys., Condens. Matter*, 11:10323–10334, 1999.
- [7] Howard F. Bates and Lewis H. Shapiro. Long-period gravity waves in ice-covered sea. *Journal of Geophysical Research*, 85(C2):1095, 1980.
- [8] D. J. Bergman. The dielectric constant of a composite material – A problem in classical physics. *Phys. Rep. C*, 43(9):377–407, 1978.
- [9] D. J. Bergman. Exactly solvable microscopic geometries and rigorous bounds for the complex dielectric constant of a two-component composite material. *Phys. Rev. Lett.*, 44:1285–1287, 1980.
- [10] D. J. Bergman. Rigorous bounds for the complex dielectric constant of a two-component composite. *Ann. Phys.*, 138:78, 1982.
- [11] M.R. Beychok. *Fundamentals of Stack Gas Dispersion: Guide*. The Author, 1994.
- [12] R. Bhattacharya. Multiscale diffusion processes with periodic coefficients and an application to solute transport in porous media. *Ann. Appl. Probab.*, 9(4):951–1020, 1999.
- [13] L. Biferale, A. Crisanti, M. Vergassola, and A. Vulpiani. Eddy diffusivities in scalar transport. *Phys. Fluids*, 7:2725–2734, 1995.
- [14] C. Bonifasi-Lista and E. Cherkaev. Electrical impedance spectroscopy as a potential tool for recovering bone porosity. 54(10):3063–3082, 2009.
- [15] B. Bowen, C. Strong, and K. M. Golden. Modeling the fractal geometry of Arctic melt ponds using the level sets of random surfaces. *Journal of Fractal Geometry*. in press.

- [16] S. R. Broadbent and J. M. Hammersley. Percolation processes I. Crystals and mazes. *Proc. Cambridge Philos. Soc.*, 53:629–641, 1957.
- [17] O. Bruno. The effective conductivity of strongly heterogeneous composites. *Proc. R. Soc. London A*, 433:353–381, 1991.
- [18] A. Bunde and S. Havlin, editors. *Fractals and Disordered Systems*. Springer-Verlag, New York, 1991.
- [19] J. T. Chayes and L. Chayes. Bulk transport properties and exponent inequalities for random resistor and flow networks. *Comm. Math. Phys.*, 105:133–152, 1986.
- [20] E. Cherkaev. Inverse homogenization for evaluation of effective properties of a mixture. *Inverse Problems*, 17(4):1203–1218, 2001.
- [21] E. Cherkaev. Spectral coupling of effective properties of a random mixture. In A. B. Movchan, editor, *IUTAM Symposium on Asymptotics, Singularities and Homogenisation in Problems of Mechanics*, volume 113 of *Solid Mechanics and Its Applications*, pages 331–340. Springer Netherlands, 2004.
- [22] E. Cherkaev and C. Bonifasi-Lista. Characterization of structure and properties of bone by spectral measure method. 44(2):345–351, 2011.
- [23] E. Cherkaev and K. M. Golden. Inverse bounds for microstructural parameters of composite media derived from complex permittivity measurements. *Waves in Random Media*, 8(4):437–450, 1998.
- [24] E. Cherkaev and M.-J. Ou. Dehomogenization: reconstruction of moments of the spectral measure of the composite. *Inverse Problems*, 24:065008 (19pp.), 2008.
- [25] E. Cherkaev and D. Zhang. Coupling of the effective properties of a random mixture through the reconstructed spectral representation. *Physica B: Condensed Matter*, 338(1–4):16–23, 2003.
- [26] K. Christensen and N. R. Moloney. *Complexity and Criticality*. Imperial College Press, London, 2005.
- [27] G. T. Csanady. Turbulent diffusion of heavy particles in the atmosphere. *J. Atmos. Sci.*, 20(3):201–208, 1963.
- [28] A. R. Day and M. F. Thorpe. The spectral function of composites: the inverse problem. *J. Phys.: Cond. Matt.*, 11:2551–2568, 1999.
- [29] G. F. Dell’Antonio and V. Nesi. A general representation for the effective dielectric constant of a composite. *J. Math. Phys.*, 29:2688, 1988.
- [30] Bernard Derrida and E Gardner. Metastable states of a spin glass chain at 0 temperature. *Journal de physique*, 47(6):959–965, 1986.

- [31] E. Di Lorenzo, D. Mountain, H. P. Batchelder, N. Bond, and E. E. Hofmann. Advances in marine ecosystem dynamics from us globec: The horizontal-advection bottom-up forcing paradigm. *Oceanography*, 26(4):22–33, 2013.
- [32] D. Dumont, A. Kohout, and L. Bertino. A wave-based model for the marginal ice zone including a floe breaking parameterization. *Journal of Geophysical Research*, 116(C4), 2011.
- [33] H. Eicken, C. Bock, R. Wittig, H. Miller, and H.-O. Poertner. Nuclear magnetic resonance imaging of sea ice pore fluids: Methods and thermal evolution of pore microstructure. *Cold Reg. Sci. Technol*, 31:207–225, 2000.
- [34] A. Fannjiang and G. Papanicolaou. Convection enhanced diffusion for periodic flows. *SIAM Journal on Applied Mathematics*, 54(2):333–408, 1994.
- [35] S. Feng, B. I. Halperin, and P. N. Sen. Transport properties of continuum systems near the percolation threshold. *Phys. Rev. B*, 35:197–214, 1987.
- [36] Colin Fox and Tim G. Haskell. Ocean wave speed in the Antarctic marginal ice zone. *Annals of Glaciology*, 33(1):350–354, jan 2001.
- [37] C. H. Fritsen, V. I. Lytle, S. F. Ackley, and C. W. Sullivan. Autumn bloom of Antarctic pack-ice algae. *Science*, 266:782–784, 1994.
- [38] K. Golden. Bounds on the complex permittivity of a multicomponent material. *J. Mech. Phys. Solids*, 34(4):333–358, 1986.
- [39] K. Golden. Convexity and exponent inequalities for conduction near percolation. *Phys. Rev. Lett.*, 65(24):2923–2926, 1990.
- [40] K. Golden. Exponent inequalities for the bulk conductivity of a hierarchical model. *Comm. Math. Phys.*, 43(3):467–499, 1992.
- [41] K. Golden and G. Papanicolaou. Bounds for effective parameters of heterogeneous media by analytic continuation. *Comm. Math. Phys.*, 90:473–491, 1983.
- [42] K. Golden and G. Papanicolaou. Bounds for effective parameters of multicomponent media by analytic continuation. *J. Stat. Phys.*, 40(5/6):655–667, 1985.
- [43] K. M. Golden. Statistical mechanics of conducting phase transitions. *J. Math. Phys.*, 36(10):5627–5642, 1995.
- [44] K. M. Golden. The interaction of microwaves with sea ice. In G. Papanicolaou, editor, *Wave Propagation in Complex Media, IMA Volumes in Mathematics and its Applications, Vol. 96*, pages 75 – 94. Springer – Verlag, 1997.
- [45] K. M. Golden. Percolation models for porous media. In U. Hornung, editor, *Homogenization and Porous Media*, pages 27 – 43. Springer – Verlag, 1997.

- [46] K. M. Golden. Climate change and the mathematics of transport in sea ice. *Notices of the American Mathematical Society*, 56(5):562–584 and issue cover, 2009.
- [47] K. M. Golden, S. F. Ackley, and V. I. Lytle. The percolation phase transition in sea ice. *Science*, 282:2238–2241, 1998.
- [48] K. M. Golden, H. Eicken, A. L. Heaton, J. Miner, D. Pringle, and J. Zhu. Thermal evolution of permeability and microstructure in sea ice. *Geophys. Res. Lett.*, 34:L16501 (6 pages and issue cover), 2007.
- [49] K. M. Golden, H. Eicken, A. L. Heaton, J. Miner, D. Pringle, and J. Zhu. Thermal evolution of permeability and microstructure in sea ice. *Geophys. Res. Lett.*, 34:L16501 (6 pages and issue cover), doi:10.1029/2007GL030447, 2007.
- [50] K. M. Golden, N. B. Murphy, and E. Cherkaev. Spectral analysis and connectivity of porous microstructures in bone. *J. Biomech.*, 44(2):337–344, 2011.
- [51] G. Grimmett. *Percolation*. Springer-Verlag, New York, 1989.
- [52] A. Gully, J. Lin, E. Cherkaev, and K. M. Golden. Bounds on the complex permittivity of polycrystalline materials by analytic continuation. *Proc. R. Soc. A*, 471(20140702), 2015.
- [53] B. I. Halperin, S. Feng, and P. N. Sen. Differences between lattice and continuum percolation transport exponents. *Phys. Rev. Lett.*, 54(22):2391–2394, 1985.
- [54] A. Herman. Numerical modeling of force and contact networks in fragmented sea ice. *Ann. Glaciol.*, 2013.
- [55] E. E. Hofmann and E. J. Murphy. Advection, krill, and antarctic marine ecosystems. *Antarctic Science*, 16(04):487–499, 12 2004.
- [56] C. Hohenegger, B. Alali, K. R. Steffen, D. K. Perovich, and K. M. Golden. Transition in the fractal geometry of Arctic melt ponds. *The Cryosphere*, 6(5):1157–1162, 2012.
- [57] M. B. Isichenko. Percolation, statistical topography, and transport in random media. *Rev. Mod. Phys.*, 64(4):961–1043, 1992.
- [58] B. Jin and W. Rundell. A tutorial on inverse problems for anomalous diffusion processes. *Inverse Problems*, 31(3):035003, 2015.
- [59] T. Jonckheere and J. M. Luck. Dielectric resonances of binary random networks. *J. Phys. A: Math. Gen.*, 31:3687–3717, 1998.
- [60] Joseph B. Keller. Gravity waves on ice-covered water. *Journal of Geophysical Research: Oceans*, 103(C4):7663–7669, apr 1998.
- [61] A. R. Kerstein. Equivalence of the void percolation problem for overlapping spheres and a network problem. *J. Phys. A*, 16:3071–3075, 1983.

- [62] A. L. Kohout, M. J. M. Williams, S. M. Dean, and M. H. Meylan. Storm-induced sea-ice breakup and the implications for ice extent. *Nature*, 509(7502):604–607, may 2014.
- [63] Pavel L Krapivsky, Sidney Redner, and Eli Ben-Naim. *A kinetic view of statistical physics*. Cambridge University Press, 2010.
- [64] D. Liu, J. Zhu, J.-L. Tison, and K. M. Golden. Inversion schemes for recovering the thermal conductivity of sea ice from temperature data. To be submitted, 2015.
- [65] Dan Lubin and Robert Massom. Sea ice. In *Polar Remote Sensing Volume I: Atmosphere and Oceans*, pages 309–728. Springer Berlin Heidelberg, 2006.
- [66] J. V. Lukovich, D. G. Babb, and D. G. Barber. On the scaling laws derived from ice beacon trajectories in the southern beaufort sea during the international polar year - circumpolar flaw lead study, 2007–2008. *J. Geophys. Res.-Oceans*, 116(C9):C00G07 (16pp.), 2011.
- [67] J. V. Lukovich, J. K. Hutchings, and D. G. Barber. On sea-ice dynamical regimes in the Arctic Ocean. *Ann. Glac.*, 56(69):323–331, 2015.
- [68] M. Luthje, D. L. Feltham, P. D. Taylor, and M. G. Worster. Modeling the summertime evolution of sea-ice melt ponds. *J. Geophys. Res.*, 111(C2):C02001, 17 pp., February 2006.
- [69] V. I. Lytle and S. F. Ackley. Heat flux through sea ice in the Western Weddell Sea: Convective and conductive transfer processes. *J. Geophys. Res.*, 101(C4):8853–8868, 1996.
- [70] C. Heussinger M. Maiti, A. Zippelius. Friction-induced shear thickening: A microscopic perspective. *Europhys. Lett.*, 2016.
- [71] A. Majda and P. R. Kramer. *Simplified Models for Turbulent Diffusion: Theory, Numerical Modelling, and Physical Phenomena*. Physics reports. North-Holland, 1999.
- [72] T. Maksym and T. Markus. Antarctic sea ice thickness and snow-to-ice conversion from atmospheric reanalysis and passive microwave snow depth. *J. Geophys. Res.*, 113:C02S12, doi:10.1029/2006JC004085, 2008.
- [73] D. McLaughlin, G. Papanicolaou, and O. Pironneau. Convection of microstructure and related problems. *SIAM J. Appl. Math.*, 45:780–797, 1985.
- [74] R. C. McPhedran, D. R. McKenzie, and G. W. Milton. Extraction of structural information from measured transport properties of composites. *Appl. Phys. A*, 29(1):19–27, 1982.
- [75] R. C. McPhedran and G. W. Milton. Inverse transport problems for composite media. *MRS Proceedings*, 195, 1 1990.

- [76] Michael H. Meylan, Luke G. Bennetts, and Alison L. Kohout. In situ measurements and analysis of ocean waves in the Antarctic marginal ice zone. *Geophysical Research Letters*, 41(14):5046–5051, jul 2014.
- [77] G. W. Milton. Bounds on the complex dielectric constant of a composite material. *Appl. Phys. Lett.*, 37:300–302, 1980.
- [78] G. W. Milton. Multicomponent composites, electrical networks and new types of continued fractions I, II. *Comm. Math. Phys.*, 111:281–327, 329–372, 1987.
- [79] G. W. Milton. *Theory of Composites*. Cambridge University Press, Cambridge, 2002.
- [80] G. W. Milton and K. Golden. Thermal conduction in composites. In T. Ashworth and David R. Smith, editors, *Thermal Conductivity 18*, pages 571 – 582. Plenum Publishing Corporation, 1985.
- [81] G. W. Milton and K. Golden. Representations for the conductivity functions of multicomponent composites. *Comm. Pure. Appl. Math.*, 43:647–671, 1990.
- [82] H. K. Moffatt. Transport effects associated with turbulence with particular attention to the influence of helicity. *Rep. Prog. Phys.*, 46(5):621–664, 1983.
- [83] Johannes E. M. Mosig, Fabien Montiel, and Vernon A. Squire. Comparison of viscoelastic-type models for ocean wave attenuation in ice-covered seas. *Journal of Geophysical Research: Oceans*, 120(9):6072–6090, sep 2015.
- [84] N. B. Murphy, E. Cherkaev, and K. M. Golden. Anderson transition for classical transport in composite materials. *Phys. Rev. Lett.*, 118:036401.
- [85] N. B. Murphy, E. Cherkaev, C. Hohenegger, and K. M. Golden. Spectral measure computations for composite materials. *Commun. Math. Sci.*, 13(4):825–862, 2015.
- [86] N. B. Murphy, E. Cherkaev, J. Zhu, J. Xin, and K. M. Golden. Spectral analysis and computation of effective diffusivities for steady random flows. 42 pp., Submitted, 2016.
- [87] N. B. Murphy, E. Cherkaev, J. Zhu, J. Xin, and K. M. Golden. Spectral analysis and computation of effective diffusivities in space-time periodic incompressible flows. *Annals of Mathematical Sciences and Applications*, 2(1):3–66, 2017.
- [88] T. Nattermann. *Spin Glasses and Random Fields*, chapter Theory of the Random Field Ising Model, page 277. World Scientific, Singapore, 1998.
- [89] CM Newman and DL Stein. Metastable states in spin glasses and disordered ferromagnets. *Physical Review E*, 60(5):5244, 1999.
- [90] M. E. J. Newman and R. M. Ziff. Efficient monte carlo algorithm and high-precision results for percolation. *Phys. Rev. Lett.*, 85:4104–4107, Nov 2000.
- [91] G. A. Pavliotis. *Homogenization theory for advection-diffusion equations with mean flow*. PhD thesis, Rensselaer Polytechnic Institute Troy, New York, 2002.

- [92] D. K. Perovich, W. B. Tucker III, and K.A. Ligett. Aerial observations of the evolution of ice surface conditions during summer. *J. Geophys. Res.*, 107(C10):doi:10.1029/2000JC000449, 2002.
- [93] D. K. Perovich and C. Polashenski. Albedo evolution of seasonal Arctic sea ice. *Geophysical Research Letters*, 39(8), 2012. L08501.
- [94] J. Klafter R. Metzler. The random walk’s guide to anomalous diffusion: A fractional dynamics approach. *Physics Reports*, (339):1–77, 2000.
- [95] P. Rampal, J. Weiss, D. Marsan, R. Lindsay, and H. Stern. Scaling properties of sea ice deformation from buoy dispersion analysis. *J. Geophys. Res.-Oceans*, 113(C3):C03002 (12pp.), 2008.
- [96] T. S. Rogers, J. E. Walsh, T. S. Rupp, L. W. Brigham, and M. Sfraga. Future Arctic marine access: analysis and evaluation of observations, models, and projections of sea ice. *The Cryosphere*, 7(1):321–332, 2013.
- [97] J. Rubinstein and S. Torquato. Flow in random porous media: Mathematical formulation variational principles, and rigorous bounds. *J. Fluid Mech.*, 206, 1989.
- [98] S. Rysgaard, J. Bendtsen, L. T. Pedersen, H. Ramløv, and R. N. Glud. Increased CO₂ uptake due to sea ice growth and decay in the Nordic Seas. *J. Geophys. Res.*, 114:C09011, doi:10.1029/2008JC005088, 2009.
- [99] M. Sahimi. *Applications of Percolation Theory*. Taylor and Francis Ltd., London, 1994.
- [100] M. Sahimi. *Flow and Transport in Porous Media and Fractured Rock*. VCH, Weinheim, 1995.
- [101] P. J. Samson. Atmospheric transport and dispersion of air pollutants associated with vehicular emissions. In A. Y. Watson, R. R. Bates, and D. Kennedy, editors, *Air Pollution, the Automobile, and Public Health*, pages 77–97. National Academy Press (US), 1988.
- [102] R. Schinzingler and P. Laura. *Conformal mapping: methods and applications*. Dover, 2003.
- [103] D. Stauffer and A. Aharony. *Introduction to Percolation Theory, Second Edition*. Taylor and Francis Ltd., London, 1992.
- [104] M. H. Stone. *Linear Transformations in Hilbert Space*. American Mathematical Society, Providence, RI, 1964.
- [105] C. Strong. Atmospheric influence on Arctic marginal ice zone position and width in the Atlantic sector, February–April 1979–2010. *Climate Dynamics*, 39:3091–3102, 2012.
- [106] C. Strong, D. Foster, E. Cherkaev, I. Eisenman, and K. M. Golden. On the definition of marginal ice zone width. *Journal of Atmospheric and Oceanic Technology*, 0(0):in press, 2017.

- [107] C. Strong and K. M. Golden. Filling the polar data gap in sea ice concentration fields using partial differential equations. *Remote Sensing*, 8(6), 2016.
- [108] C. Strong and K. M. Golden. Filling the sea ice data gap with harmonic functions. *SIAM News*, 50, 2017.
- [109] Courtenay Strong and Ignatius G. Rigor. Arctic marginal ice zone trending wider in summer and narrower in winter. *Geophys. Res. Lett.*, 40(18):4864–4868, September 2013.
- [110] G. I. Taylor. Diffusion by continuous movements. *Proc. London Math. Soc.*, 2:196–211, 1921.
- [111] D. N. Thomas and G. S. Dieckmann, editors. *Sea Ice, 2nd Edition*. Wiley-Blackwell, Oxford, 2009.
- [112] C. J. Thompson. *Classical Equilibrium Statistical Mechanics*. Oxford University Press, Oxford, 1988.
- [113] S. Torquato. *Random Heterogeneous Materials: Microstructure and Macroscopic Properties*. Springer-Verlag, New York, 2002.
- [114] S. Torquato and D. C. Pham. Optimal bounds on the trapping constant and permeability of porous media. *Phys. Rev. Lett.*, 92:255505:1–4, 2004.
- [115] S. Torquato and J. Rubinstein. Diffusion-controlled reactions. II. Further bounds on the rate constant. *J. Chem. Phys.*, 90:1644–1647, 1989.
- [116] Takenobu Toyota, Christian Haas, and Takeshi Tamura. Size distribution and shape properties of relatively small sea-ice floes in the Antarctic marginal ice zone in late winter. *Deep Sea Research Part II: Topical Studies in Oceanography*, 58(9-10):1182–1193, may 2011.
- [117] Y. A. Vetter, J. W. Deming, P. A. Jumars, and B. B. Krieger-Brockett. A predictive model of bacterial foraging by means of freely released extracellular enzymes. *Microb. Ecol.*, 36:75–92, 1998.
- [118] Peter Wadhams. *Ice in the Ocean*. Gordon and Breach Science Publishers, London, 2000.
- [119] Ruixue Wang and Hayley H. Shen. Gravity waves propagating into an ice-covered ocean: A viscoelastic model. *Journal of Geophysical Research*, 115(C6), June 2010.
- [120] W. M. Washington and C. L. Parkinson. *An Introduction to Three-dimensional Climate Modeling*. University Science Books, 1986.
- [121] E. Watanabe and H. Hasumi. Pacific water transport in the western Arctic Ocean simulated by an eddy-resolving coupled sea ice–ocean model. *J. Phys. Oceanogr.*, 39(9):2194–2211, 2009.

- [122] W. F. Weeks and A. Assur. Fracture of lake and sea ice. Research Report 269, USA CRREL, Hanover, NH, 1969.
- [123] M. G. Worster and D. W. Rees Jones. Sea-ice thermodynamics and brine drainage. *Phil. Trans. R. Soc. A*, 373:20140166, 2015.
- [124] D. Zhang and E. Cherkaev. Reconstruction of spectral function from effective permittivity of a composite material using rational function approximations. *J. Comput. Phys.*, 228(15):5390–5409, 2009.